Wear, Volumes 418-419, January 2019, pp. 102-110
DOI:10.1016/j.wear.2018.11.010

Micro-impact testing of AlTiN and TiAlCrN coatings

Ben D. Beake[1,*], Luis Isern[2], Jose L. Endrino[2] and German S. Fox-Rabinovich[3]

1 Micro Materials Ltd, Willow House, Yale Business Village, Ellice Way, Wrexham, LL13 7YL, UK

2 SEPi (Surface Engineering & Precision Institute), School of Aerospace, Transport and Manufacturing, Cranfield University, Bedford, MK43 0AL, UK

3 Department of Mechanical Engineering, McMaster University, 1280 Main Street West, Hamilton, Ontario L8S 4L7, Canada

*Corresponding author: Tel: +44 1978 261615; e-mail: ben@micromaterials.co.uk

Keywords: micro-impact; fracture resistance; PVD; AlTiN; TiAlCrN

Abstract

A novel micro-scale repetitive impact test has been developed to assess the fracture resistance of hard coatings under dynamic high strain rate loading. It is capable of significantly higher impact energies than in the nano-impact test. It retains the intrinsic depth-sensing capability of the nano-impact test enabling the progression of the damage process to be monitored throughout the test, combined with the opportunity to use indenters of less sharp geometry and still cause rapid coating failure. The micro-impact test has been used to study the resistance to impact fatigue of Al-rich PVD nitride coatings on cemented carbide. The impact fatigue mechanism has been investigated in nano- and micro-scale impact tests. Coating response was highly load-dependent. A $Ti_{0.25}Al_{0.65}Cr_{0.1}N$ coating with high H^3/E^2 performed best in the nano- and micro- impact tests although it was not the hardest coating studied. The

role of mechanical properties, microstructure and thickness on impact behaviour and performance in cutting tests is discussed.

1. Introduction

Al-rich PVD nitride coatings have been developed with dense nanocrystalline or columnar microstructures, high oxidation resistance, very good elevated temperature mechanical properties, low thermal conductivity at elevated temperature and potential for tribological adaptability through formation of complex tribo-films [1-30]. Consequently, they have shown excellent performance in machining aerospace alloys such as Ni-based superalloys (Inconel 718, Waspaloy, ME16) [10,13,18], titanium alloys [7,9,18], and other hard-to-cut materials such as hardened steel [4,14,15,17], stainless steel [8] and super duplex stainless steel [30]. To enhance their performance further, advanced coating characterisation techniques can improve our fundamental understanding of the link between coating properties and durability in cutting so that their coating architectures can be optimised [6,22,23,31]. Accordingly, multi-scale, multi-technique mechanical/tribological characterisation is increasingly becoming an integral tool in streamlining the development of advanced wear resistant coatings. By performing nano- and micro-scale mechanical and tribological tests with different probe geometry, applied loads, test temperatures, contact geometry, static and repetitive loading it is possible to change the position of the peak stresses in contact and more closely simulate the actual contact conditions.

Under the tribologically extreme contact conditions in metal cutting, a key requirement enabling the coating to protect the carbide substrate is resistance to fracture. Nanoindentation can be used to assess toughness as a measure of resistance to crack initiation and overload failure, but it is not possible to monitor crack propagation under repetitive, oscillating loading

conditions in the standard quasi-static nanoindentation test [23]. The dynamic, high strain rate repetitive nano-impact test is a suitable alternative. The high strain rate contact in this test can provide much closer simulation of the performance of coatings systems under highly loaded intermittent contact and the evolution of wear under these conditions. In practice, studies have reported a strong correlation between fracture resistance in the nano-impact test and cutting tool life. For example, Bouzakis and co-workers investigated the influence of the developed compressive stresses during micro-blasting on the brittleness of $Ti_{40}Al_{60}N$ coated cemented carbide by performing nano-impact tests. They reported a correlation between the results of the nano-impact tests and the cutting performance when milling hardened steel (AISI 4140) [32]. Lower impact depth at the end of the test (high impact resistance) was strongly correlated with longer cutting tool life, and trends in tool life with micro-blasting pressure were well reproduced by the nano-impact test. The relative ranking of cutting performance after micro-blasting with ZrO_2 and Al_2O_3 at a given pressure and the switch in relative performance between 0.2-0.4 MPa were also well reproduced in the impact test data [32].

Higher H^3/E^2, a measure of resistance to plastic deformation, commonly results in improved resistance to fracture initiation due to enhanced load support. H^3/E^2 has also been taken as a direct measure of fracture resistance [28]. Bartosik and co-workers have recently reported a strong correlation between H^3/E^2 and the fracture toughness determined from cantilever bending experiments on annealed AlTiN coatings [29]. Coatings with very high H^3/E^2 have shown improved resistance to erosion by solid particle impact (erodent 50 μm Al_2O_3) [33, 34]. Hassani and co-workers noted that although very hard coatings were predisposed to brittle failure, maximising the H^3/E^2 ratio could be achieved by reducing elastic modulus whilst maintaining an optimal hardness to provide the best combination of resistance to

plastic deformation and resistance to brittle failure [34]. Hassani et al. used finite element calculation to show that, for monolayer coatings, the combination of low elastic modulus and high thickness could reduce maximum tensile stress and potentially improve erosion resistance [35]. Finite element modelling results have suggested that, for multi-layer coatings with graded properties, a significant reduction in tensile stress could be achieved by increasing the elastic modulus closer to the coating-substrate interface [36]. Studies have shown that Al-rich (>50 at.%) (Ti,Al)N-based coatings display enhanced fracture resistance and are more durable in nano-impact testing. Even a small increase in Al:Ti ratio can result in greater resistance to cracking and lower final impact wear depths than TiN [37] or $Ti_{0.50}Al_{0.50}N$ [25]. Resistance to repetitive nano-impact of 8 μm $Al_{0.54}Ti_{0.46}N$ coatings with varying through-thickness multilayered microstructure was improved by increasing the number of layers [38]. In more complex Al-rich coatings, impact resistance was improved in multilayered TiAlCrSiYN/TiAlCrN with higher H^3/E^2 in comparison to monolayered TiAlCrSiYN coatings with lower H^3/E^2 [3,13,14]. Higher H^3/E^2 can result in more abrupt failures in repetitive tests. This has been investigated in monolayer TiAlCrSiYN and in TiAlCrSiYN/TiAlCrN with 55-60% Al [13]. Grain size decreases in TiAlCrSiYN multilayers at higher Al %. Monolayers and multilayers with higher Al fraction were more susceptible to fracture, but it occurred more gradually.

By changing the applied load and probe geometry in the impact test, it is possible to alter the severity of the test and to move the positions of peak impact-induced stresses relative to the coating-substrate interface. Chen and co-workers studied the behaviour of multilayer TiAlSiN and monolayer TiN coatings on hardened tool steel in nano-impact tests with a cube corner probe at 10-150 mN [39]. A higher load was required for chipping in the multilayered TiAlSiN coating though they found no delamination on either coating throughout the load

range. The improved performance of the TiAlSiN coating tested in that study was considered to be due to a combination of microstructural (less columnar with multilayer structure to aid crack deflection) and mechanical (higher H^3/E^2) advantages over the monolayered columnar TiN.

Although it is relatively easy to fracture hard and tough PVD coatings with the nano-impact test when sharp cube corner probes are used, when blunter probe geometries are used it is not usually possible to cause rapid fracture on these types of samples. Therefore, it is desirable to increase the energy delivered per impact so that different indenter geometries can be used instead. Torres and co-workers have noted that, by switching from sharp to blunter spherical indenters, there is an intrinsic suitability for examining damage evolution in bulk materials as a function of number of cycles [40] and it is possible to assess fatigue sensitivity. Qiu and co-workers have argued that very large radius probes are less suited for coating systems as the peak stresses are well into the substrate [41-42]. They, therefore, developed a repeated indentation test using a 200-micron radius probe and applied loads in the range 90-300 N. Although the test was not fully instrumented, so that it was necessary to stop it to observe deformation, they were able to show enhanced sensitivity to differences in adhesion strength due to changing interlayers [41-42].

In the current work, we report the first results with a new impact test capable of impact loads in the micro- range (~0.5-5 N). The energy supplied per impact is the product of the impact load and accelerating distance. The maximum energy supplied per impact with the micro-impact technique is around 2 orders of magnitude greater than the maximum possible in the nano-impact technique. It retains the intrinsic depth-sensing capability of the nano-impact test enabling the progression of the wear process to be monitored throughout the test, combined

with the opportunity to use probes of less sharp geometry. The use of blunter probes prolongs the life of the tip and reduces the requirement of monitoring probe sharpness, simplifying the testing. Bouzakis and co-workers noted that, whilst many impact studies have focussed on fracture initiation, the subsequent film damage propagation is also important, as it relates to the ability of the coating to withstand loads after fatigue damage initiation [43]. In these tests without depth-sensing capability, it was necessary to stop the test periodically and employ averaged properties such as the failed area ratio to follow the evolution of damage process with time, which is not necessary in the micro-impact test.

To investigate the suitability of the micro-impact test technique for evaluating hard coatings tests were performed on three Al-rich (>50 at.%) (Ti,Al)N-based coatings that have been shown to perform well in metal cutting applications [10,25,44]. AlTiN has previously been shown to be resistant to fracture in the nano-impact test [25], and TiAlCrN has higher hot hardness and oxidation resistance [44]. The coatings were also characterised by nanoindentation, micro-scratch, micro-wear and nano-impact test techniques. By performing micro- and nano-impact tests over a range of impact forces on the same coatings, it has been possible to contrast the deformation mechanisms operative in the tests due to the different loading conditions.

2. Experimental

2.1 Coating deposition

$Ti_{0.1}Al_{0.7}Cr_{0.2}N$ and $Ti_{0.25}Al_{0.65}Cr_{0.1}N$ coatings were deposited on mirror polished H10A cemented carbide WC-Co substrates from $Ti_{0.1}Al_{0.7}Cr_{0.2}$ and $Ti_{0.25}Al_{0.65}Cr_{0.1}$ powder metallurgical targets respectively in an R&D-type hybrid PVD coater (Kobe Steel Ltd.) using a plasma-enhanced arc source. Samples were heated up to about 500 °C and cleaned by Ar

ion etching. Ar-N_2 gas was fed to the chamber at a pressure of 2.7 Pa with a N_2 partial pressure of 1.3 Pa. The arc source was operated at 100 A for a 100 mm diameter x 16 mm thick target. The $Al_{0.67}Ti_{0.33}N$ coating was synthesized using an Oerlikon Balzers' Rapid Coating System (RCS) in a cathodic arc ion-plating mode. During the deposition, the chamber was back-filled with a pure reactive nitrogen atmosphere and the pressure was in the range 1-4 Pa. The substrates had 3-fold rotation and were heated to a temperature of ~600 °C, with an average substrate bias of −100 V. For simplicity, the $Ti_{0.1}Al_{0.7}Cr_{0.2}N$, $Ti_{0.25}Al_{0.65}Cr_{0.1}N$ and $Al_{0.67}Ti_{0.33}N$ coatings are hereafter referred to as TiAl70CrN, TiAl65CrN and AlTiN respectively. The target coating thickness was (2.0 ± 0.5) μm. R_a surface roughness was ~0.06 μm for the AlTiN and TiAl70CrN and ~0.17 μm for the TiAl65CrN. The grain size is ~5 nm in AlTiN and ~20 nm in TiAl70CrN [18]. XPS studies of electronic structure have shown that AlTiN has more metallic character than TiAl70CrN where bonding is closer to metal-covalent [18]. The coatings have predominantly TiN-based fcc crystal structure, with solid solution of Al or (Al,Cr) [18]. AlTiN has more wurtzite h-AlN. Relatively small changes in the PVD conditions can alter the grain size, columnar character and mechanical properties of AlTiN with the same chemical composition [12]. The elastic modulus of the AlTiN studied here is higher than those reported in other studies [26-28], consistent with less dual-phase h-AlN in the tested coating.

2.2 Nanomechanical and micro-scratch characterisation

Nanoindentation, micro-scratch, nano- and micro-impact tests were performed with a NanoTest system (Micro Materials Ltd, Wrexham, UK). Nanoindentation was performed with a Berkovich diamond indenter. The instrument was fully calibrated for load, displacement, frame compliance and indenter shape according to an ISO14577-4 procedure. The area function for the indenter was determined by indentation into a fused silica reference

sample. For the nanoindentation of the coatings, a peak load of 40 mN was chosen to minimize the influence of the relatively high surface roughness on the data whilst ensuring that the indentation contact depth was under 1/10 of the film thickness so that a coating-only (load-invariant) hardness could be measured in combination with coating-dominated elastic modulus. Due to the high surface roughness, 40 indentations were performed on each coating. Hardness and reduced elastic modulus were determined from power-law fitting to the unloading curves. The elastic modulus and Poisson ratio of the diamond indenter were 1141 GPa and 0.07 respectively. The reduced indentation moduli were converted to Elastic moduli assuming a Poisson ratio for both coatings of 0.25. The micro-scratch tests were performed as topography-scratch-topography scans with a 25 μm end radius diamond probe. In all scans, the scanning speed was 5 μm/s, and the scratch track length was 800 μm. In the ramped scratch scan after a 200 μm levelling distance, the load was ramped at 100 mN/s to 12 N. Three repeat tests were performed on each coating. Three repetitive constant load (multi-pass wear) tests were also performed. After an initial topographic (pre-wear surface profile) scan, in scans 2-11 the load was ramped to 2 N and kept at this level until the end of the test. Residual deformation after the 10-cycle wear test was assessed by a final topographic (post-wear surface profile) scan. The variation in the mean depth and friction averaged over the constant load region of the scratch track was recorded to assess the number of cycles required for coating failure.

2.3 Nano- and micro-impact tests

Nano-impact testing was performed with a NanoTest fitted with a cube corner indenter as an impact probe. The indenter was accelerated from 10 μm above the coating surface with 50-150 mN impact load to produce an impact every 4 s for 300 or 600 seconds (75 or 150 impacts). The coatings' resistance to impact fatigue was assessed by following the

progression of the impact depth with continued impacts. The nano-impact tests were performed with two diamond cube corner indenters, which differed in their end radius (a new, sharp ~50-100 nm tip, and an older tip, which had become blunter through wear ~150 nm). 10 repeat 600 s tests were performed at 150 mN with the well-used cube corner on all three coatings. Tests with the sharper probe were performed at 50-150 mN on the two better performing coatings, AlTiN and TiAl65CrN. There were 7 repeat 300 s tests at 50 mN and 5 repeat 600 s tests at 100 and 150 mN.

To enable micro-impact tests to be performed, the high load head of a NanoTest Vantage was extended below the indenter position. This adapted loading head was actuated with a large electromagnet capable of pulling the probe at least 50 μm away from the sample surface. A spheroconical diamond indenter with nominal end radius of 25 μm was used as an impact probe. Calibration on fused silica showed the actual radius was ~17 μm. Repeat micro-impact tests were performed at 0.75-2.5 N with a constant accelerating distance of 40 μm. The test duration was 300 s with 1 impact every 4 s, resulting in 75 impacts in total. There were 3 repeats at each load which were separated by 200 μm. SEM imaging (using an FEI XL30 ESEM at 20 kV and a working distance of 6 - 8 mm) and EDX analysis (Oxford instruments and Aztec software) was performed on micro-scratch tracks, micro-wear tracks and micro-impact craters. Confocal Laser Scanning Microscopy of the micro-impact craters was also carried out using an Olympus Lext OLS3100 on areas of 128 μm x 96 μm.

3. Results

3.1 Nanoindentation, micro-scratch and micro-wear

The mechanical properties from the nanoindentation tests and the critical load from the micro-scratch tests are summarised in Table 1. The mechanical properties of the three

coatings are similar with H ~ 25-28 GPa and E ~ 440 GPa. The resistance to plastic deformation, H^3/E^2, was highest on the TiAl65CrN and lowest on the TiAl70CrN. The critical load for coating cracking (L_{c1}) in the micro-scratch test was similar on all three coatings but there were clear differences in the L_{c2} coating failure. This was highest on the TiAl65CrN and lowest on the TiAl70CrN. For all of the coatings, the friction coefficient at failure was ~0.13-0.15 in the progressive load micro-scratch test (Figure 1).

The SEM imaging revealed tensile (cohesive) arc cracking prior to total (cohesive+adhesive) coating failure for all three coatings. Figure 2 (a-b) shows the secondary electron (SE) and back-scattered (BS) images of coating failure on the TiAl65CrN coating. The BS image shows that substrate exposure occurred to the sides of the scratch track at coating failure. The increase in load between the onset of the cracking and total failure (L_{c2}-L_{c1}) was greater for the TiAl65CrN coating. For the other two coatings, substrate exposure was also observed in the scratch track, initially periodically, with smaller chipping and substrate exposure outside the track (as illustrated in figure 2 (c-d) for TiAl70CrN).

In the repetitive micro-scratch tests at 2 N, the variation in mean on-load scratch depth (Figure 3) and measured friction force with number of scratch passes were monitored to determine the number of cycles to coating failure. 2 N is close to the L_{c2} critical load for the TiAl70CrN and this coating already started to fail in the first scratch pass. With subsequent scratches on this coating, the friction coefficient increased from an initial value of 0.16. On the AlTiN and TiAl65CrN coatings, several scratches were required before the coating started to fail. Coating failure initially occurred over isolated regions of the 500 μm long region of the track at 2 N. With continued scratch passes, progressively more of the scratch track exhibited coating failure. In the tests shown in Fig. 3, AlTiN started to fail over a

significant fraction of the scratch track on the sixth pass and TiAl65CrN on the 8th. Similar results were obtained in the other repeat tests on these coatings. For the AlTiN and TiAl65CrN coatings, the difference in depth before and after coating failure provides an estimate of coating thickness which was 2.0 and 2.5 μm respectively. For these two coatings, the friction coefficient reduced to ~0.08 at failure before increasing thereafter. For the TiAl70CrN, the thickness from confocal microscopy was 1.6 μm. BS imaging showed that there were greater chipping and substrate exposure outside the wear track for the coating which failed more abruptly in the test, TiAl65CrN, than on the other two coatings.

3.2 Nano-impact testing

It was not possible to produce coating failure in nano-impact tests with the less sharp cube corner indenter on the TiAl65CrN or AlTiN coatings in 600 s at 150 mN, although the TiAl70CrN failed within a few impacts (figure 4). With the sharper probe, the TiAl65CrN or AlTiN coatings did not fail in most 300 s tests at 50 mN either but failed at higher load. The typical results shown in figure 5 suggest that the failure mechanism differed between these two coatings. There was a shorter time-to-failure for the AlTiN with a more gradual, progressive increase in impact depth thereafter. In contrast, on the TiAl65CrN the initial failure required more impacts and was more abrupt. Table 2 summarises the failure behaviour and impact depth data after 300 s and 600 s. The TiAl65CrN was more resistant, but once failure occurred, there was little difference in impact depth.

3.3. Micro-impact testing

All three coatings showed a strong dependence on impact load as illustrated for TiAl65CrN in figure 6. The impact load required to cause coating failure within the 300 s test varied between the coatings as summarised in Table 3. TiAl70CrN was the least impact resistant,

with failure occurring in 1/3 tests at 0.75 N and all tests at 1.0 N. TiAl65CrN was most impact resistant, with no failures to 1.25 N and only one failure at 1.5 N. AlTiN exhibited no failures at 0.75 N, but failed in some tests at 1.0-1.5 N. At 1.75 N all coatings failed in every test. The variation in the (on-load) impact depth through the duration of the test is shown in figure 7 (a-c), with one example shown from each impact load. Confocal microscopy of impact craters revealed little elastic recovery in the impact depth after the load removal. An example comparison at 1.25 N is shown in figure 8. During the first few impacts all three coatings showed similar behaviour, but with continuing impact clear differences emerged. After ~100 s (25 impacts), the TiAl70CrN begins to fail, and after further impacts, a more gradual failure was also seen for the AlTiN, but the TiAl65CrN was resistant to the end of the test.

When there is no chipping of the coating, little or no change in impact depth with repetitive impacts was found after the first few impacts. Confocal microscopy showed, however, that ring cracks were present even for tests where chipping was absent (figure 9). BS images of impact craters (e.g. figure 6) confirm that no substrate exposure occurs in any impact tests where the depth did not increase significantly after the first impacts. Confocal microscopy showed slight pile-up around the impact craters in some tests where substrate exposure did not occur, with more significant debris displaced above the original surface being observed at the edge of the impact crater in tests where there was coating chipping and substrate exposure. SE and BS images show that the predominant coating failure occurs around the periphery of the impact crater, as illustrated for TiAl65CrN in figure 10. There was some chipping extending beyond this region, but it did not reach the substrate. EDX analysis confirms the periphery is largely composed of elements from the exposed substrate. In the central region of the impact crater the coating was still present, but with additional elements

from the WC-Co substrate also found, due to coating wear. A transition to a faster wear rate was observed in the latter part of most the tests at >2 N on the AlTiN and TiAl65CrN samples which resulted in greater final impact depth. EDX analysis of the central region of the impact craters showed that it was largely composed of W, C and Co and the coating was completely removed from this region. However, BS images showed that when this transition was not observed in the impact depth data, the coating was still present in this central region.

4. Discussion

The novel micro-impact test was effective in causing failure of the hard PVD coatings in short test duration. The behaviour of the coatings in the test is highly load-dependent as shown in Table 3. Figure 11 shows how the mean depth after (a) one impact and (b) at the end of the test varies across the load range for the three coatings. The repetitive micro-impact tests show excellent reproducibility in the mean depth after a single impact and also in the mean depth at the end of the test when fracture does not occur in any of the repeat tests at that load. When fracture does occur in some of the repeat tests this results in greater variability in the time to failure and the final depth, i.e. the test displays a typical stochastic response for a fracture-dominated process. In terms of resistance to a single impact, there was no difference between any of the coatings across the entire load range. However, the final depth data after 75 impacts correlate with the impact fracture data presented in Table 3, with TiAl70CrN being the least fracture resistant and TiAl65CrN the most resistant when subjected to multiple impact. The influence of coating microstructure, mechanical properties and thickness on this behaviour is discussed more detail in section 4.3. At >2 N all the coatings failed, but the final depth on TiAl70CrN was not as great as for AlTiN or TiAl65CrN. TiAl70CrN is more closely modulus matched with substrate, which may be beneficial in hindering crack propagation [45]. Micro-impact tests at 1.5 and 2.5 N on the uncoated substrate have shown

that it has better crack resistance than the coatings under these conditions. Lower final impact depth on the TiAl70CrN at 2.25 and 2.5 N may, therefore, be related to its lower thickness. Apart from this switch in behaviour at the highest loads, the three coatings showed the same relative ranking in the nano- and micro- impact tests, although there were some differences in degradation mechanism, which are discussed in more detail in the following sections.

4.1 Micro-impact deformation mechanism

By examining the impact depth vs time plots and SE and BS images of impact craters, it is possible to determine the general features of impact-fatigue mechanism on these PVD coatings on cemented carbide substrate. The deformation proceeds through 4 distinct stages as the test progresses:

Stage 1. During the initial impacts, the WC-Co substrate yield stress is exceeded, and the impact depth increases until the stress in the contact decreases due to plastic deformation and increased contact area. Ring cracking may occur (as in Figure 9), but radial cracks are absent.

Stage 2. Once the contact size has increased to the point that the substrate no longer yields, there is minimal change in impact depth with each successive impact. Provided the coating does not start to chip, this cyclic impact fatigue continues through the test. In some tests, there was a very small depth decrease with continued impacts, due to work hardening of the coating, which may be implicated in the onset of coating damage. The highest stresses are at the periphery of the contact. Fatigue damage is most significant here, as is commonly observed in radial fretting contacts. The stress distribution is a function of load, coating thickness and mechanical properties. On each impact, the coating has to bend significantly to

accommodate the substrate elastic (and plastic) deformation, increasing the likelihood of cracking.

Stage 3. The impact depth starts to increase as the coating begins to become damaged by cracking. The joining up of these cracks ultimately leads to coating removal [38,46]. With continued impact, there is a transition to a more pronounced wear process involving through-thickness cracking and/or large chipping events and more rapid increase in probe depth. EDX data show this involves coating failure and substrate exposure around the periphery of the impact crater.

Stage 4. In the final stage, the damage tolerance of the failed coated system controls the wear behaviour. At higher load (≥ 2 N) after a larger number of impacts, there is a transition to a total coating failure where the coating is completely removed. This leads to a second period of more rapid depth increase in the micro-impact test.

4.2 Length scale effects - contrasting deformation in nano- and micro-impact tests

Figure 12 shows typical examples of higher load nano- and micro-impact tests on the TiAl65CrN after frame compliance correction to compare the evolution of impact depth in both types of test. In these examples the number of repetitive impacts required for failure (18 and 20) was quite similar in both tests. The failure is more abrupt, with the depth increasing more rapidly over a smaller number of cycles in the nano-impact test with the sharp cube corner probe. Chipping outside of the impact crater is the predominant failure mode for nitride coatings in the nano-impact test [18,39,50,51]. TEM of FIB x-sections through impact craters showed that on TiAlSiN cracks begin in the coating and no delamination was observed [39]. 3D-FEM simulations of nano-impact tests on 3 μm $Al_{60}Ti_{40}N$ and various

multilayer and monolayer $Al_{54}Ti_{46}N$ 8 μm PVD coatings deposited on cemented carbide inserts with cube corner diamond indenters also focussed on coating degradation [38,46]. The model calculated the von Mises stress in the impact region. When the maximum stress between nodes exceeded the rupture stress, these nodes become disconnected and crack formation is simulated. In this way, it was possible to reproduce the experimental load dependence of impact fatigue and its initiation and evolution with continued impacts.

Whilst it was possible to interpret the behaviour in the nano-impact by focussing on the coating behaviour alone, in the micro-impact test it is important to consider the composite response of the coating and substrate. The depth at failure is greater in the micro-impact test due to greater elastic deformation of the substrate and coating bending to accommodate this. Finite element analysis has shown that changing the ratio between coating thickness h and indenter radius R can influence the dominant failure mechanisms in deformation of a coated system by a spherical indenter [52]. The h/R ratio varies between the micro- and nano-impact tests. Taking the effective radius for the cube corner indenter as at least a few hundred nm at the relevant penetration depths, gives h/R ~1-10 in nano-impact and ~0.1-0.15 in micro-impact. These differences influence the deformation mechanism. In contrast to the chipping without delamination observed in nano-impact, in the micro-impact the chipping is accompanied by substrate exposure and degradation of the hard WC at the periphery of the impact crater. The advantages of the micro-impact test lie in its ability to (1) use probes of less sharp geometry, which are more durable than sharper probes, and still cause rapid coating failure due to the higher impact energy (2) use different h/R to investigate the role of the substrate on the coating degradation mechanism.

4.3 Influence of mechanical properties on impact resistance

A complex relationship exists between coating mechanical properties and impact resistance. As previously shown [22], the interplay between coating mechanical properties, thickness and microstructure determine impact resistance. In coatings with very high H^3/E^2, materials dissipative mechanisms such as localised plasticity to minimise strain accumulation are necessarily more limited. To optimise coating durability, a structural advantage is beneficial, such as multi-layering, grain refinement/suppression of weak columnar boundaries or introduction of a sub-layer. In the TiAl65CrN coating, the combination of higher H^3/E^2 and greater thickness confers benefits, but there is no accompanying microstructural advantage, so more extensive chipping was observed in micro-scratch testing. The denser nanocrystalline AlTiN has a microstructural advantage in comparison to the columnar TiAlCrN coatings by virtue of removing columnar boundaries which can be detrimental to crack propagation. The differences between AlTiN and TiAl65CrN in the nano-impact tests with the sharper probe are consistent with differences in H^3/E^2 and in plasticity. As the variation in H^3/E^2 between the three coatings is relatively small differences in coating thickness may also play a role. Musil has shown that increasing coating thickness in hard coating systems on soft substrates increases the resistance to circular cracking on indentation [53-55]. However, the substrate in the current study, H10A cemented carbide, is stiffer and, at ~23 GPa, almost as hard as the nitride coatings. In a recent study, a 1.3 μm AlTiN showed significantly better impact resistance than a 3.6 μm AlCrN coating [17]. Despite differences in contact geometry in the scratch and impact tests, the relative performance of the three coatings is the same in both types of test. The higher H^3/E^2 and coating thickness are beneficial in providing greater load support resulting in higher critical load and cycles to failure in the micro-scratch test and resistance to impact-fatigue in the impact test. Chipping outside the impact crater or scratch track is more extensive for the coating with the highest H^3/E^2. In the repetitive scratch test, the reduction in friction with number of scratch passes is due to an initial smoothing out of

asperities and reduction in ploughing component until the coatings failed whereupon the friction increases as in the ramped load scratches. This increase in friction is due to increased contact area from ploughing and contact with debris at the sides of the track as observed with increasing load in the ramped scratch test.

5. Conclusions

The novel micro-scale impact test is capable of significantly higher impact energies than in nano-impact which results in rapid failure of PVD coatings when impacted with a spheroconical diamond probe with 17-micron end radius. The response of the TiAl65CrN, TiAl70CrN and AlTiN coatings deposited on cemented carbide was strongly load-dependent. The coating performance in the nano- and micro-impact tests, and in micro-scale scratch and wear tests, was influenced by a combination of their mechanical properties, microstructure and thickness. The coating with highest H^3/E^2, TiAl65CrN, performed best in the nano- and micro- impact tests, although it was not the hardest coating studied. There are some similarities and differences in the impact fatigue mechanism in nano- and micro-scale impact tests due to the different stress distributions involved. Failure on repetitive impact with a sharp cube corner probe in the nano-impact test was by coating chipping, whilst in the micro-impact test with the spherical probe, cracking was accompanied by debonding around the periphery of the contact and substrate fatigue

6. Acknowledgements

The funding to develop the novel micro-impact test technique through the Innovate UK Project No: 132369 – “Nano-to Micro-Impact Testing: An in-situ test for UK SEAC sector”

is gratefully acknowledged. Nick Pickford and Dr Stephen Goodes (both Micro Materials Ltd.) are acknowledged for modifying the NanoTest hardware and software respectively to develop the new micro-impact capability.

7. References

1. G. Erkens, R. Cremer, T. Hamoudi, K.-D. Bouzakis, I. Mirisidis, S. Hadjiyiannis, G.Skordaris, A. Asimakopoulos, S. Kombogiannis, J. Anastopoulos and K. Efstathiou, Properties and performance of high aluminium containing (Ti,Al)N based supernitride coatings in innovative cutting applications, Surf. Coat. Technol. 177-178 (2004) 727-734.
2. W. Kalss, A. Reiter, V. Derflinger, C. Gey and J.L. Endrino, Modern coatings in high performance cutting applications, Int. J. Refract. Met. Hard Mater. 24 (2006) 399-404.
3. G.S. Fox-Rabinovich, J.L. Endrino, M.H. Agguire, B.D. Beake, S.C. Veldhuis, A.I. Kovalev, I.S. Gershman, K. Yamamoto, Y. Losset, D.L. Wainstein and A.Y. Rashkovskiy, Mechanism of adaptability for the nano-structured TiAlCrSiYN-based hard physical vapor deposition coatings under extreme frictional conditions, J. Appl. Phys. 111 (2012) 064306.
4. G.S. Fox-Rabinovich, S.C. Veldhuis, G.K. Dosbaeva, K. Yamamoto, A.I. Kovalev, D.L. Wainstein, I.S. Gershman, L.S. Shuster and B.D. Beake, Nanocrystalline coating design for extreme applications based on the concept of complex adaptive behaviour, J. Appl. Phys. 103 (2008) 083510.
5. K. Kutschej, P.H. Mayrhofer, M. Kathrein, P. Polcik, R. Tessadri and C. Mitterer, Structure, mechanical and tribological properties of sputtered coatings with $Ti_{1-x}Al_xN$ ($0.5 \leq x \leq 0.75$) Surf. Coat. Technol. 200 (2005) 2358-2365.

6. K.-D. Bouzakis, N. Michailidis, G. Skordaris, E. Bouzakis, D. Biermann, R. M'Saoubi, Cutting with coated tools: coating technologies, characterization methods and performance optimisation, CRIP Ann. Manuf. Technol. 61 (2012) 703-723.
7. Hultman, L. and Mitterer, C. (2006) Nanostructured coatings Cavaleiro, A. and De Hosson, J.Th.M. eds. Chapter 11, "Thermal stability of advanced nanostructured wear-resistant coatings" (Springer, New York) pp464-510.
8. J.L. Endrino, G.S. Fox-Rabinovich, C. Gey, Hard AlTiN, AlCrN PVD coatings for machining of austenitic stainless steel, Surf. Coat. Technol. 200 (2006) 6840-6845.
9. N. Michailidis, Variations in the cutting performance of PVD-coated tools in milling Ti6Al4V, explained through temperature-dependent coating properties, Surf. Coat. Technol. 304 (2016) 325-329.
10. G.S. Fox-Rabinovich, K. Yamamoto and A.I. Kovalev, (2007) Self-organization during friction: Advanced surface engineered materials and systems design, G.S. Fox-Rabinovich, G. Totten (eds.) Chapter 10 "Synergistic alloying of self-adaptive wear-resistant coatings" pp297-334, (Taylor and Francis Books/CRC Press LLC, USA).
11. A. Hörling, L. Hultman, M. Odén, J. Sjölén, L. Karlsson, Mechanical properties and machining performance of $Ti_{1-x}Al_xN$-coated cutting tools, Surf. Coat. Technol. 191 (2005) 384-392.
12. J.M. Anderson, J. Vetter, J. Müller, J. Sjölén, Structural effects of energy input growth of $Ti_{1-x}Al_xN$ ($0.55 \leq x \leq 0.66$) coatings by cathodic arc evaporation, Surf. Coat. Technol. 240 (2014) 211-220.
13. G.S. Fox-Rabinovich, B.D. Beake, K. Yamamoto, M.H. Aguirre, S.C. Veldhuis, G. Dosbaeva, A. Elfizy, A. Biksa, and L.S. Shuster, A.Y. Rashkovskiy, Structure, properties and wear performance of nano-multilayered TiAlCrSiYN/TiAlCrN

coatings during machining of Ni-based aerospace superalloys, Surf Coat Technol 204 (2010) 3698-3706.

14. G.S. Fox-Rabinovich, K. Yamamoto, B.D. Beake, A.I. Kovalev, M.H. Aguirre, S.C. Veldhuis, G.K. Dosbaeva, D.L. Wainstein, A. Biksa and A.Y. Rashkovskiy, Emergent behavior of nano-multilayered coatings during dry high speed machining of hardened tool steels, Surf. Coat. Technol. 204 (2010) 3425-3435.
15. K.-D. Bouzakis, S. Hadjiyiannis, G. Skordaris, I. Mirisidis, N. Michailidis, K. Efstathiou et al, The effect of coating thickness, mechanical strength and hardness properties on the milling performance of PVD coated cemented carbide inserts, Surf. Coat. Technol. 177-178 (2004) 657-664.
16. A. Inspektor and P.A. Salvador, Architecture of PVD coatings for metalcutting applications: a review, Surf. Coat. Technol. 257 (2014) 138-153.
17. B.D. Beake, L. Ning, C. Gey, S.C. Veldhuis, A. Komarov, A. Weaver, M. Khanna, G.S. Fox-Rabinovich, Wear performance of different PVD coatings during wet end milling of H13 tool steel, Surf. Coat. Technol. 279 (2015) 118-125.
18. G.S. Fox-Rabinovich, S.C. Veldhuis, K. Yamamoto, MH. Aguirre, A. Kovalev, D.L. Wainstein, B.D. Beake, J.L. Endrino, D.L. Wainstein, A.Y. Rashkovskiy, Design and performance of AlTiN and TiAlCrN PVD coatings for machining of hard to cut materials, Surf. Coat. Technol. 204 (2009) 489-496.
19. L. Chen, J. Paulitsch, Y. Du and P.H. Mayrhofer, Thermal stability and oxidation resistance of Ti-Al-N coatings, Surf. Coat. Technol. 206 (2012) 2954-2960.
20. M.H. Staia, M. D'Alessandria, D.T. Quinto, F. Roudet, M. Marsal Astort, High-temperature tribological characterisation of commercial TiAlN coatings, J. Phys.: Condens. Matter 18 (2006) S1727-S1736.

21. E. Le Bourhis, P. Goudeau, M.H. Staia, E. Carrasquero, E.S. Puchi-Cabrera, Mechanical properties of hard AlCrN-based coated substrates, Surf. Coat. Technol. 203 (2009) 2961-2968.
22. B.D. Beake, G.S. Fox-Rabinovich, Progress in high temperature nanomechanical testing of coatings for optimising their performance in high speed machining, Surf. Coat. Technol. 255 (2014) 1021115.
23. B.D. Beake, G.S. Fox-Rabinovich, S.C. Veldhuis, S.R. Goodes, Coating optimisation for high-speed machining with advanced nanomechanical test methods, Surf. Coat. Technol., 203 (2009) 1919-1925.
24. G.S. Fox-Rabinovich, B.D. Beake, S.C. Veldhuis, J.L. Endrino, R. Parkinson, L.S. Shuster, M.S. Migranov, Impact of mechanical properties measured at room and elevated temperatures on wear resistance of cutting tools with TiAlN and AlCrN coatings, Surf. Coat. Technol. 200 (2006) 5738-5742.
25. B.D. Beake, J.F. Smith, A. Gray, G.S. Fox-Rabinovich, S.C. Veldhuis and J.L. Endrino, Investigating the correlation between nano-impact fracture resistance and hardness/modulus ratio from nanoindentation at 25-500ºC and the fracture resistance and lifetime of cutting tools with $Ti_{1-x}Al_xN$ (x = 0.5 and 0.67) PVD coatings in milling operations, Surf. Coat. Technol. 201 (2007) 4585-4593.
26. G.S. Fox-Rabinovich, J.L. Endrino, B.D. Beake, M.H. Aguirre, S.C. Veldhuis, D.T. Quinto, C.E. Bauer, A.I. Kovalev and A. Gray, Effect of annealing below 900°C on structure, properties and tool life of an AlTiN coating under various cutting conditions, Surf. Coat. Technol. 202 (2008) 2985-2992.
27. G.S. Fox-Rabinovich, J.L. Endrino, B.D. Beake, A.I. Kovalev, S.C Veldhuis, L. Ning, F. Fotaine and A. Gray, Impact of annealing on the microstructure, properties, and cutting performance of AlTiN coating, Surf. Coat. Technol. 201 (2006) 3524-3529.

28. Y.X. Xu, H. Riedl, D. Holec, L. Chen, Y. Du and P.H. Mayrhofer, Thermal stability and oxidation resistance of sputtered Ti-Al-Cr-N hard coatings, Surf. Coat. Technol. 324 (2017) 48-56.
29. M. Bartosik, C. Rumeau, R. Hahn, Z.L. Zhang and P.H. Mayrhofer, Fracture toughness and structural evolution in the TiAlN system upon annealing, Sci. Rep. 7 (2017) 16476.
30. Y.S. Ahmed, J.M. Paiva, D. Covelli and S.C. Veldhuis, Investigation of coated cutting tool performance during machining of super duplex stainless steels through 3D wear evaluations, Coatings 7 (2017) 127 15pp (doi:10.3390/coatings7080127).
31. M. Tkadletz, N. Schalk, R. Daniel, J. Keckes, C. Czettl, C. Mitterer, Advanced characterisation methods for wear resistant hard coatings: a review on recent progress, Surf. Coat. Technol. 285 (2016) 31-46.
32. K.-D. Bouzakis, F.Flocke, G. Skordaris, E. Bouzakis, S. Geradis, G. Katirtzoglou and S. Makrimallakis, Influence of dry micro-blasting grain quality on wear behaviour of TiAlN coated tools, Wear 271 (2011) 783-791.
33. S. Hassani, M. Bielawski, W. Beres, L. Martinu, M. Balazinski and J.E. Klemberg-Sapieha, Predictive tools for the design of erosion resistant coatings, Surf. Coat. Technol. 203 (2008) 204-210.
34. E. Bousser, M. Benkahoul, L. Martinu and J.E. Klemberg-Sapieha, Effect of microstructure on the erosion resistance of Cr-Si-N coatings, Surf. Coat. Technol. 203 (2008) 776-780.
35. S. Hassani, J.E. Klemberg-Sapieha, M. Bielawski, W. Beres, L. Martinu and M. Balazinski, Design of hard coating architecture for the optimisation of erosion resistance, Wear 265 (2008) 879-887.

36. S. Hassani, M. Bielawski, W. Beres, M. Balazinski, L. Martinu and J.E. Klemberg-Sapieha, Impact stress absorption and load spreading in multi-layered erosion-resistant coatings, Wear 268 (2010) 770-779.
37. J. Chen, H. Li and B.D. Beake, Load sensitivity in repetitive nano-impact testing of TiN and AlTiN coatings, Surf. Coat. Techol. 308 (2016) 289-297.
38. G. Skodaris, K.-D. Bouzakis, P. Charalampous, A dynamic FEM simulation of the nano-impact test on mono- or multi-layered PVD coatings considering their graded strength properties determined by experimental-analytical procedures, Surf. Coat. Technol. 265 (2015) 53-61.
39. J. Chen, R. Ji, R.H.U. Khan, X. Li, B.D. Beake and H. Dong, Effects of mechanical properties and layer structure on the cyclic loading of TiN-based coatings Surf. Coat. Technol. 206 (2011) 522-529.
40. E. Torres, G. Ramirez, Y. Gaillard, E. Jimenez-Pique and L. Llanes, Contact fatigue behaviour of PVD-coated hardmetals, Int. J. Refract. Met. Hard Mater. 27 (2009) 323-341.
41. L.S. Qiu, X.D. Zhu, S. Lu, G.Y. He and K.W. Xu, Quantitative evaluation of bonding strength for hard coatings by interfacial fatigue strength under cyclic indentation, Surf. Coat. Technol. 315 (2017) 303-313.
42. L. Qiu, X. Zhu, G. He and K. Xu, The repeated spherical indentation test: an efficient way to evaluate the adhesion of hard coatings, Surf. Eng. 32 (2016) 578-584.
43. K.-D. Bouzakis, A. Siganos, T. Leyendecker and G. Erkens, Thin hard coatings fracture propagation during the impact test, Thin Solid Films 460 (2004) 181-189.
44. G.S. Fox-Rabinovich, K. Yamamoto, S.C. Veldhuis, A.I. Kovalev and G.K. Dosbaeva, Tribological adaptability of TiAlCrN PVD coatings under high performance dry machining conditions, Surf. Coat. Technol. 200 (2005) 1804-1813.

45. J.C.A. Batista, C. Godoy, G. Pintaude, A. Sinatora, A. Matthews, An approach to elucidate the different response of PVD coatings in different tribological tests, Surf. Coat. Technol. 174–175 (2003) 891-898.
46. K.-D. Bouzakis, S. Gerardis, G. Skordaris and E. Bouzakis, Nano-impact tests on a TiAlN PVD coating and correlation between experimental and FEM results, Surf. Coat. Technol., 206 (2011) 1936-1940.
47. K.-D. Bouzakis, P. Charalampous, G. Skordaris, F. Dimofte, N.M. Ene, R. Ehinger, S. Gardner, B.S. Modrzejewski and J.R. Fetty, Fatigue and adhesion characterisation of DLC coatings on steel substrates by perpendicular and inclined impact tests, Surf. Coat. Technol. 275 (2015) 207-213.
48. N. Norrby, M. P. Johansson, R. M'Saoubi, M. Odén, Pressure and temperature effects on the decomposition of arc evaporated Ti0.6Al0.4N coatings in continuous turning, Surf. Coat. Technol. 209 (2012) 203-207.
49. K.-D. Bouzakis, M. Pappa, E. Bouzakis, G. Skordaris and S. Gerardis, Correlation between PVD coating strength properties and impact resistance at ambient and elevated temperatures Surf. Coat. Technol., 205 (2010) 1481.
50. A. Mosquera, L. Mera, G. S. Fox-Rabinovich, R. Martínez, I. Azkona, and J. L. Endrino, Advantages of Nanoimpact Fracture Testing in Studying the Mechanical Behavior of CrAl(Si)N Coatings, Nanoscience and Nanotechnology Letters, Vol. 2, 352–356, 2010.
51. A. Mosquera, L. Mera, G. S. Fox-Rabinovich, R. Martínez, I. Azkona, and J. L. Endrino, Statistical Analysis of Nanoimpact testing of Hard CrAl(Si)N Coatings, Mater. Res. Soc. Symp. Proc. 2011: p. 1339.

52. J. Michler, E. Blank, Analysis of coating fracture and substrate plasticity induced by spherical indentors: diamond and diamond-like carbon layers on steel substrates, Thin Solid Films 381 (2001) 119-134.
53. J. Musil and M. Jirout, Toughness of hard nanostructured ceramic thin films, Surf. Coat. Technol. 201 (2007) 5148-5152.
54. M. Jirout and J. Musil, Effect of addition of Cu into ZrOx film on its properties, Surf. Coat. Technol. 200 (2006) 6792-6800.
55. J. Musil, Advanced hard coatings with enhanced toughness and resistance to cracking, Chapter 7, pp378-463 in Thin Films and Coatings: Toughening and Toughness Characterisation, ed. S Zhang, CRC Press, July 2015, p383.

Tables

Table 1 nanoindentation and micro-scratch results

	H (GPa)	E (GPa)	H/E	H^3/E^2 (GPa)	L_{c1} (N)	L_{c2} (N)
AlTiN	25.6 ± 4.9	413 ± 58	0.062	0.099	1.2 ± 0.2	2.9 ± 0.4
TiAl65CrN	27.8 ± 1.5	445 ± 87	0.062	0.108	1.4 ± 0.1	4.6 ± 0.2
TiAl70CrN	27.5 ± 6.5	467 ± 62	0.059	0.095	1.2 ± 0.1	2.1 ± 0.1

Table 2 Nano-impact results on TiAl65CrN and AlTiN with sharper cube corner

	Applied Load (mN)	Impact depth at 300 s (μm)	Failure at 300 s*	Impact depth at 600 s (μm)	Failure at 600 s
AlTiN	50	1.6 ± 0.8	1/7		
	100	3.7 ± 0.2	5/5	4.1 ± 0.2	5/5
	150	4.4 ± 0.2	5/5	4.8 ± 0.2	5/5
TiAl65CrN	50	1.1 ± 0.1	0/7		
	100	2.4 ± 0.8	3/5	3.5 ± 1.2	4/5
	150	4.2 ± 0.5	5/5	4.7 ± 0.4	5/5

* The tests at 50 mN were stopped after 300 s.

Table 3 Load dependence of number of micro-impact tests showing coating failure and substrate exposure

	Impact force (N)							
	0.75	1.0	1.25	1.5	1.75	2.0	2.25	2.5
AlTiN	0/3	1/3	2/3	1/3	3/3	3/3	3/3	3/3
TiAl65CrN	0/3	0/3	0/3	1/3	3/3	3/3	3/3	3/3
TiAl70CrN	1/3	3/3	3/3	3/3	3/3	3/3	3/3	3/3

Figure captions

1. Friction coefficient vs. load in progressive load micro-scratch tests.

2. SEM images of the coating failure in the micro-scratch test. a) SE image on TiAl65CrN. b) BS image on TiAl65CrN c) SE image of TiAl70CrN d) BS image of TiAl70CrN.

3. Evolution of the on-load scratch depth with number of scratches in repetitive micro-scratch tests at 2 N.

4. Nano-impact tests at 150 mN with the blunter probe.

5. Nano-impact tests at 50-150 mN with the sharper cube corner probe. (a) TiAl65CrN (b) AlTiN.

6. SE (top) and BS (bottom) SEM images of impact craters on TiAl65CrN at impact forces of 750 mN (furthest left), 1000 mN, 1250 mN, 1750 mN, 2000 mN and 2250 mN (furthest right). No substrate is visible for tests at 1250 mN or lower.

7. Example micro-impact test depth vs. time data over the load range 750-2500 mN (a) TiAl65CrN (b) AlTiN (c) TiAl70CrN.

8. Comparative micro-impact test results on each coating at 1250 mN.

9. Confocal micrograph of impact craters showing ring cracking. (a) TiAl70CrN 750 mN (b) AlTiN 1500 mN (c) TiAl65CrN 1000 mN.

10. SE (left) and BS (right) SEM images of an impact crater on TiAl65CrN at 1750 mN.

11. Load dependence of initial (a) and final (b) impact depth.

12. Comparison of the evolution of damage on TiAl65CrN in (a) nano-impact with the sharp cube corner and (b) micro-impact with the R = 17 μm spherical probe.

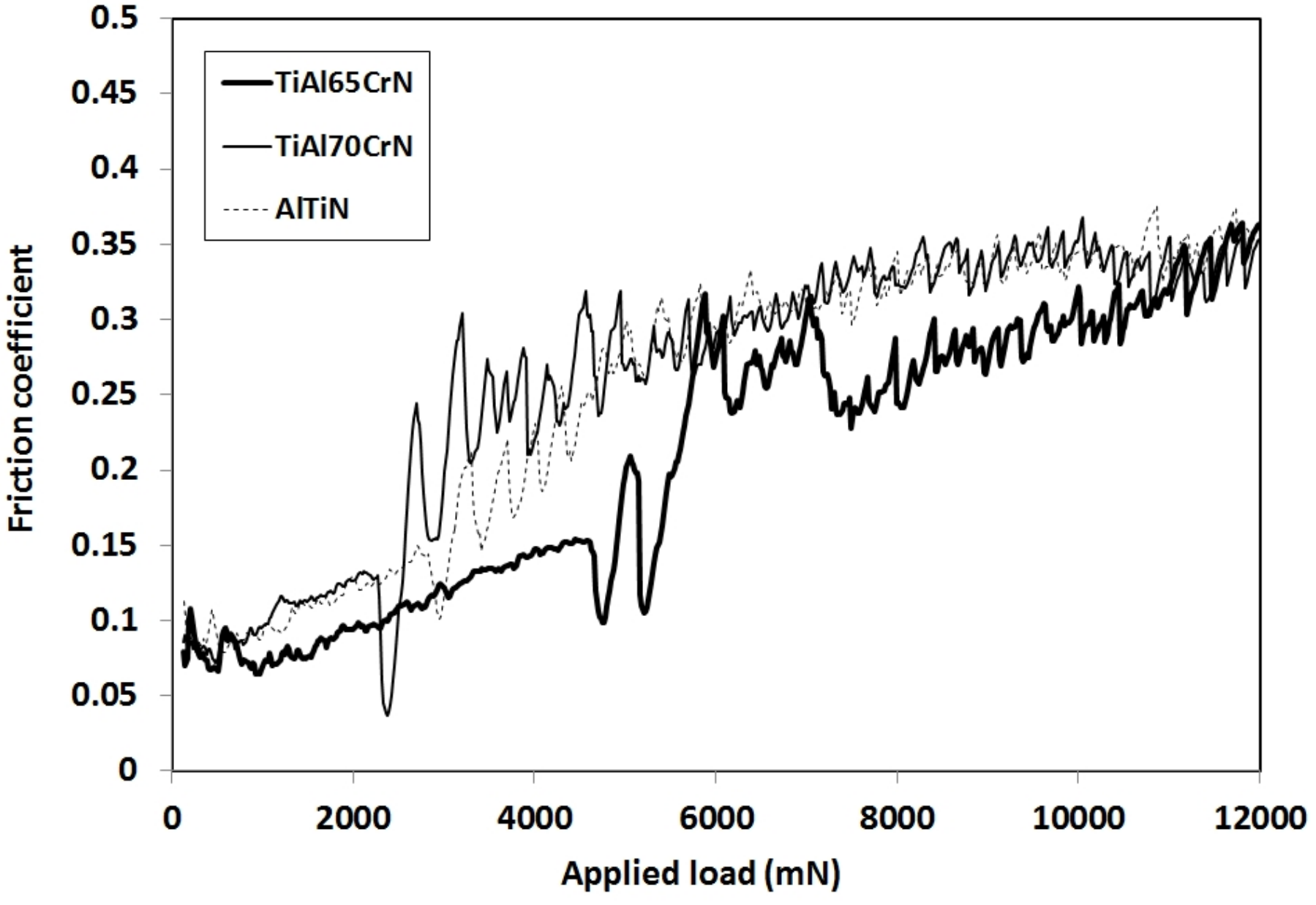
TiAl65CrN
TiAl70CrN
AlTiN
Friction coefficient
0.5
0.45
0.4
0.35
0.3
0.25
0.2
0.15
0.1
0.05
0
0
2000
4000
6000
8000
10000
12000
Applied load (mN)

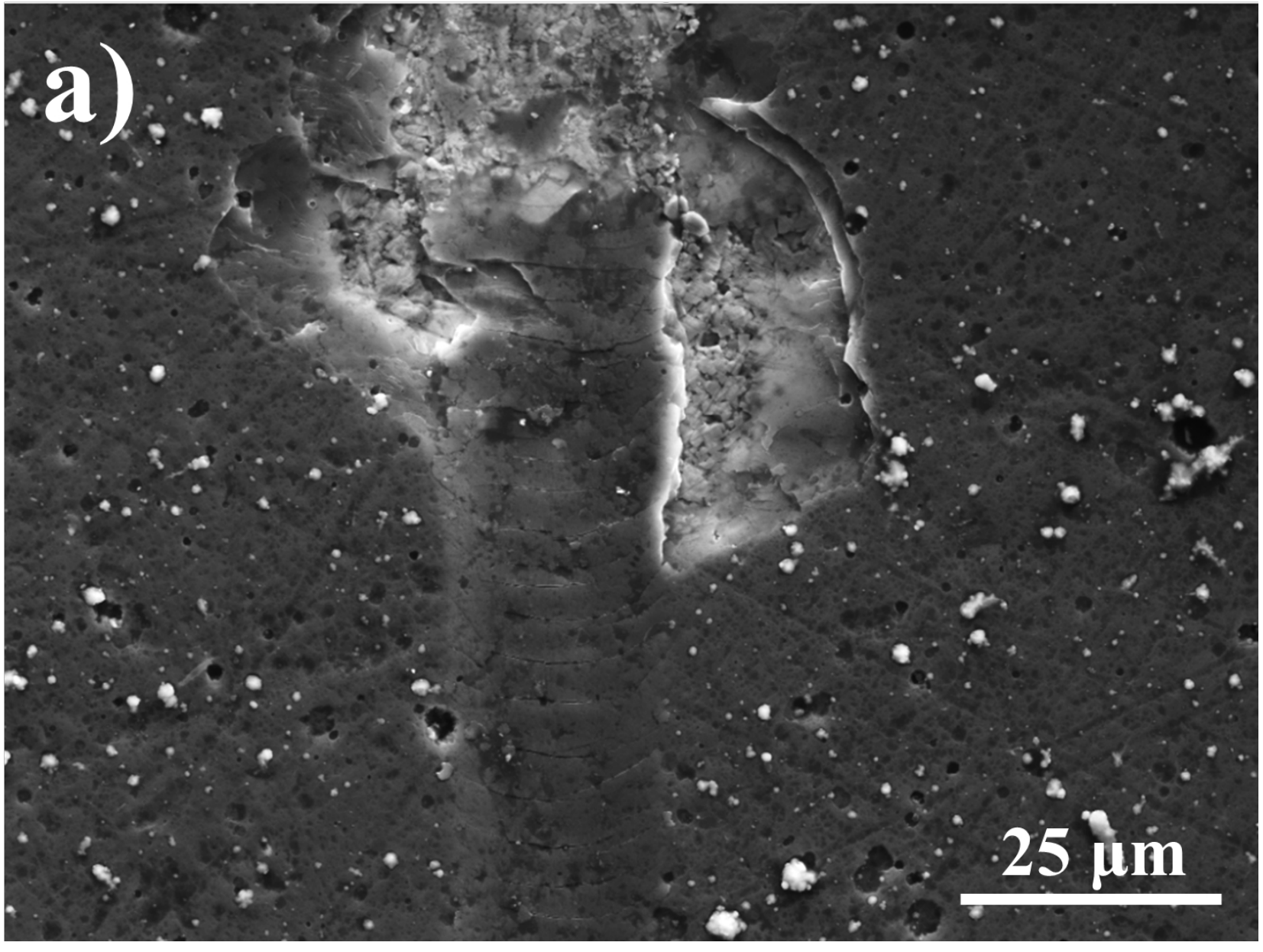
a)
25 µm

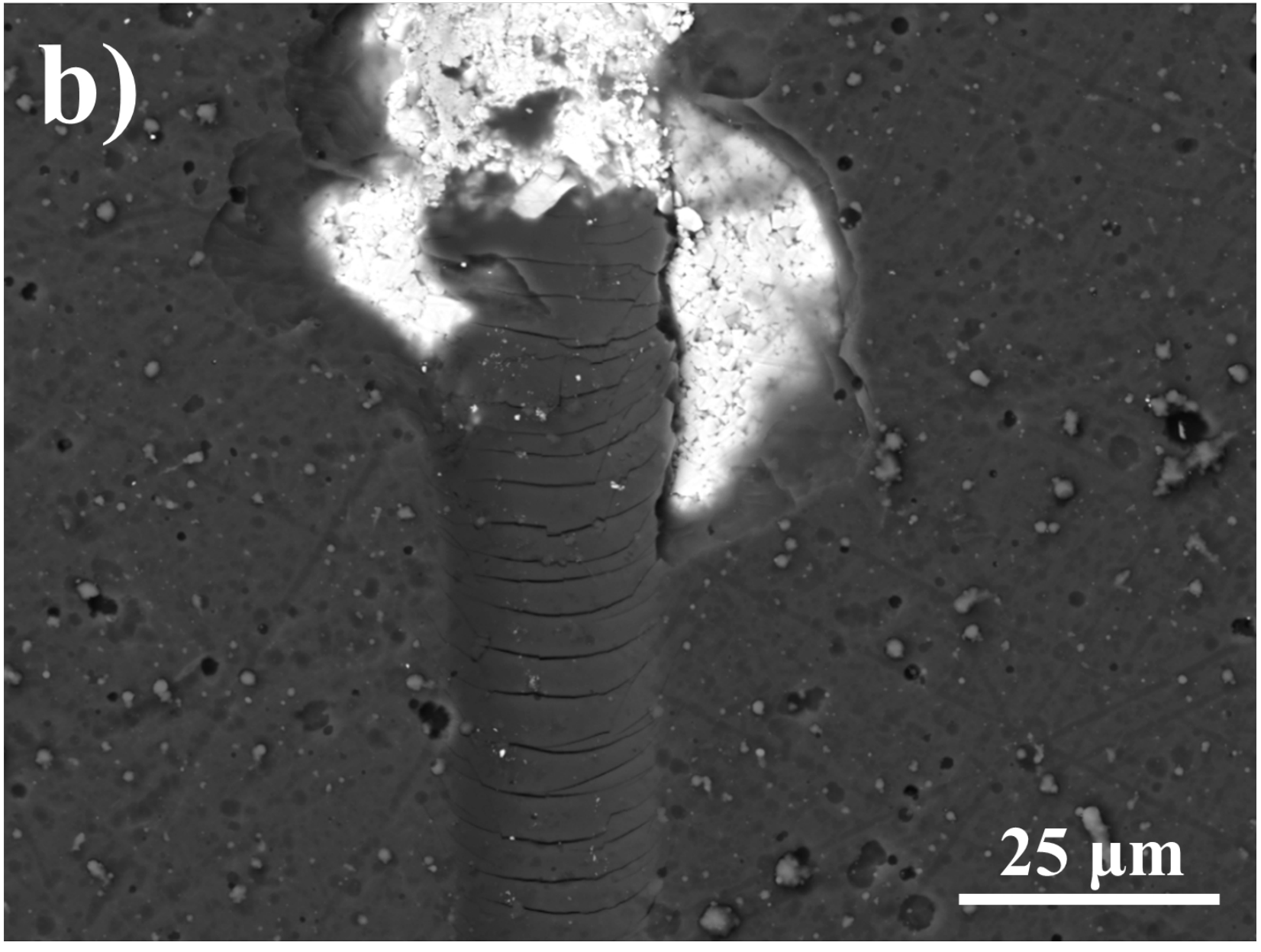
b)
25 µm

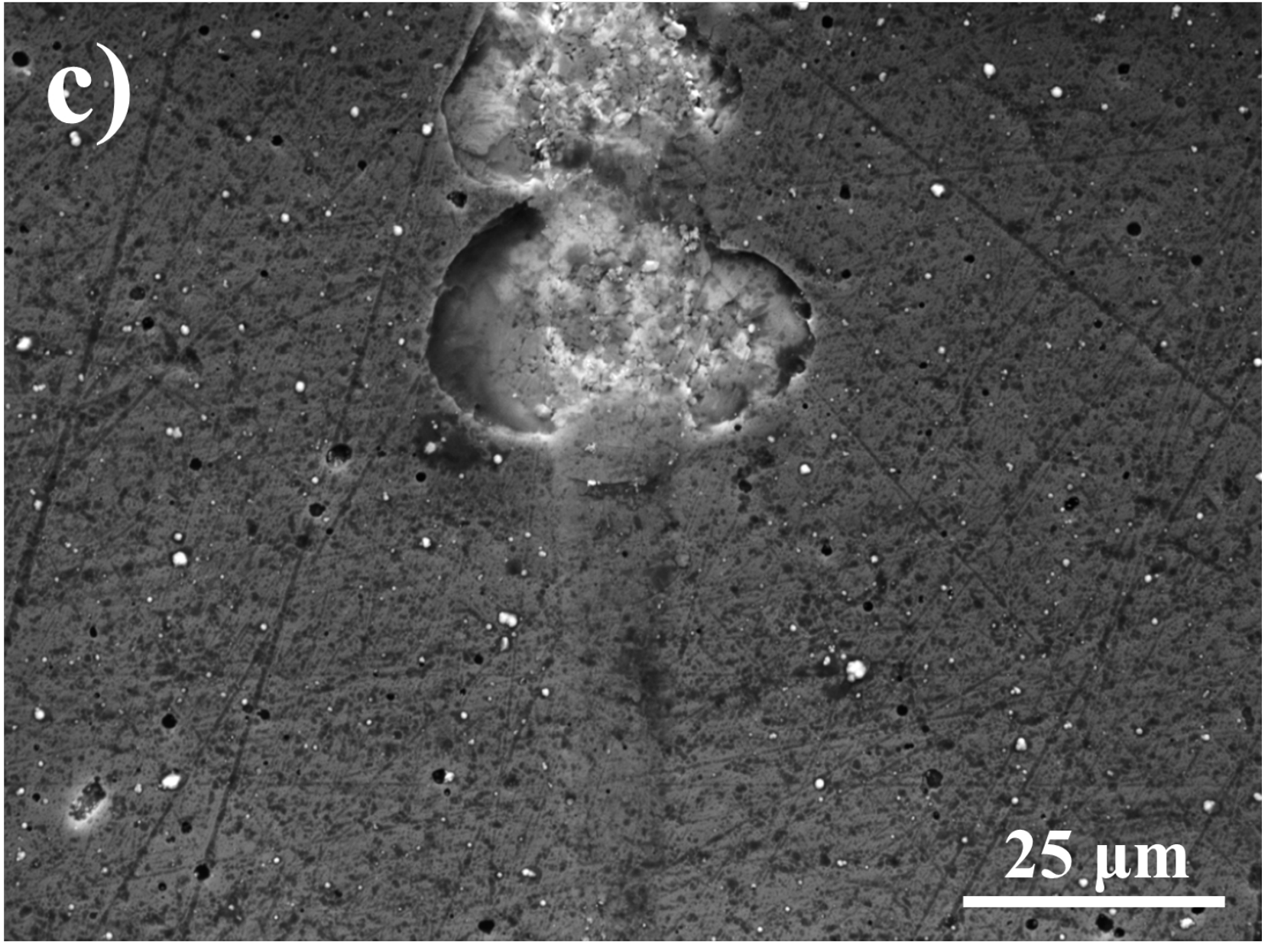
c)
25 µm

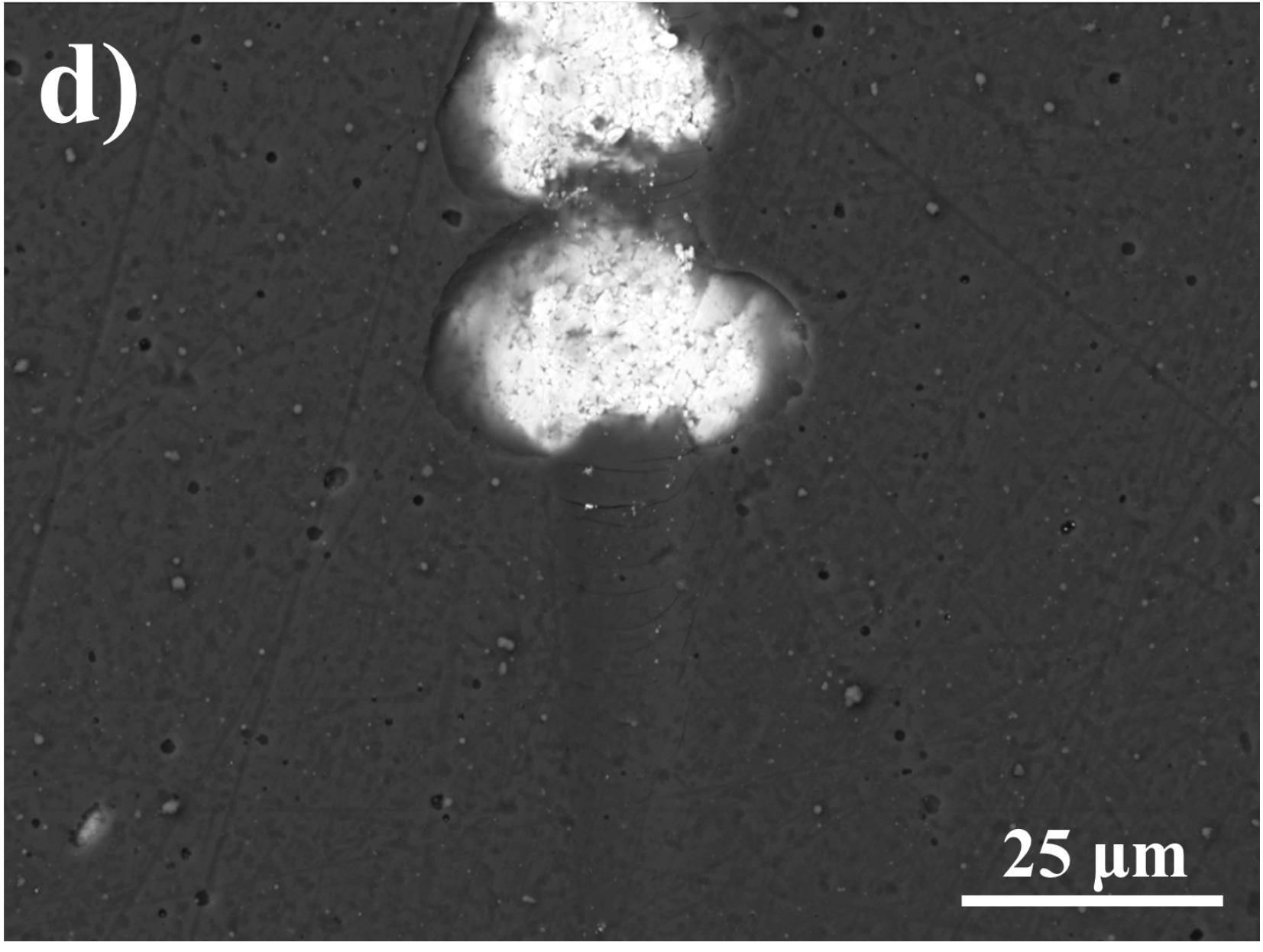
d)
25 µm

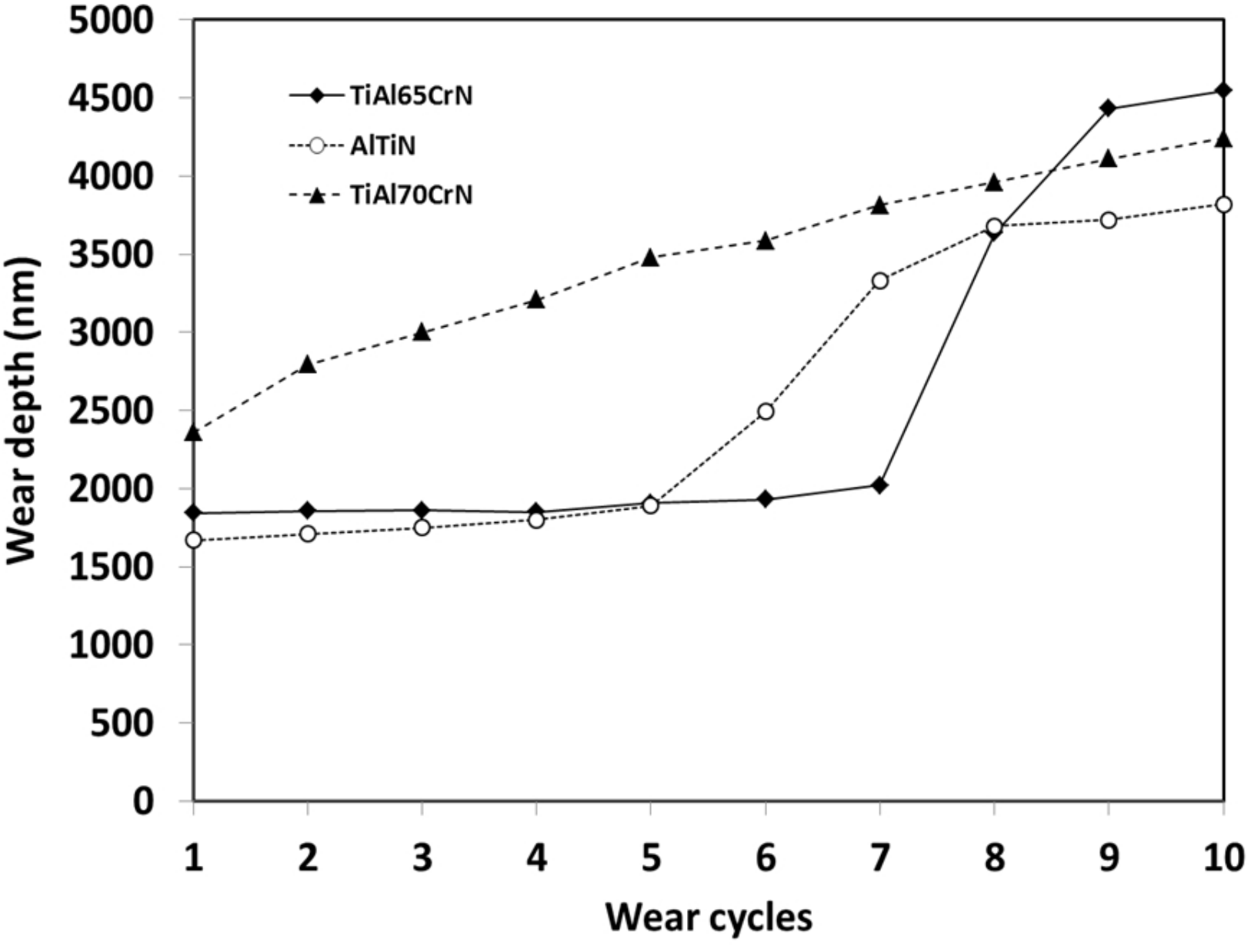
5000
4500
4000
3500
3000
2500
2000
1500
1000
500
0
Wear depth (nm)
TiAl65CrN
AlTiN
TiAl70CrN
1
2
3
4
5
6
7
8
9
10
Wear cycles

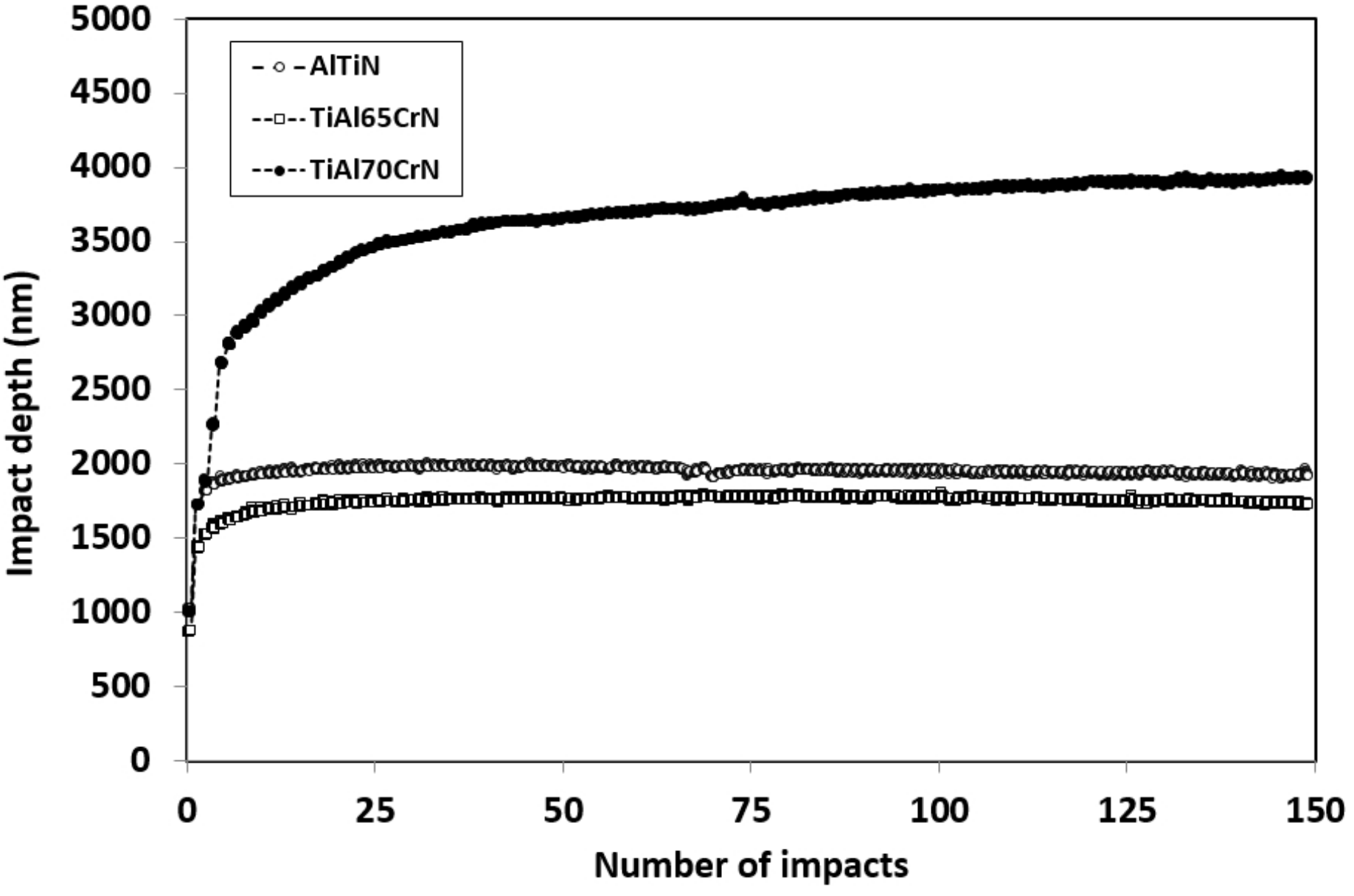
AlTiN
TiAl65CrN
TiAl70CrN
Impact depth (nm)
5000
4500
4000
3500
3000
2500
2000
1500
1000
500
0
0
25
50
75
100
125
150
Number of impacts

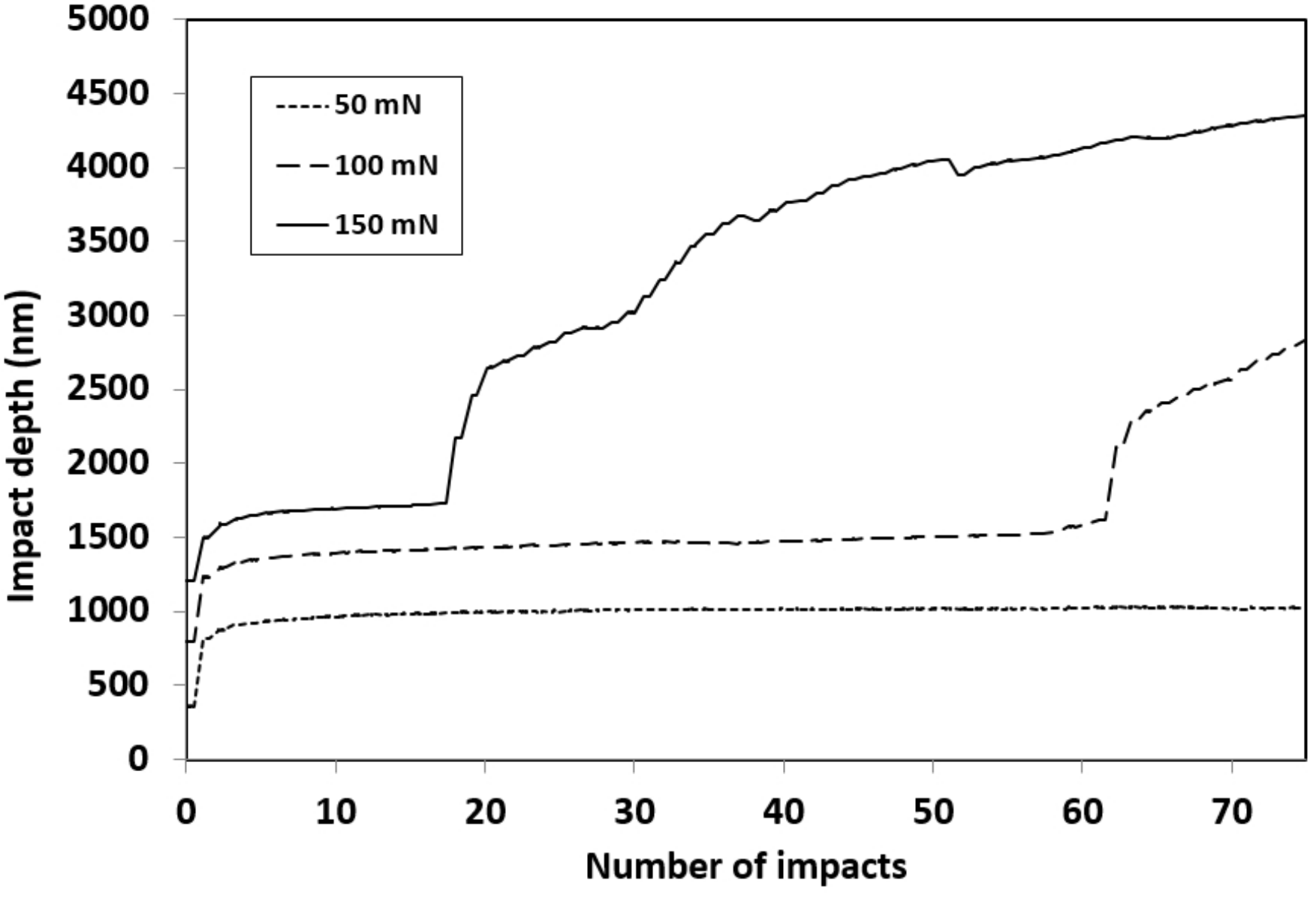
5000
4500
4000
3500
3000
2500
2000
1500
1000
500
0
Impact depth (nm)
50 mN
100 mN
150 mN
0
10
20
30
40
50
60
70
Number of impacts

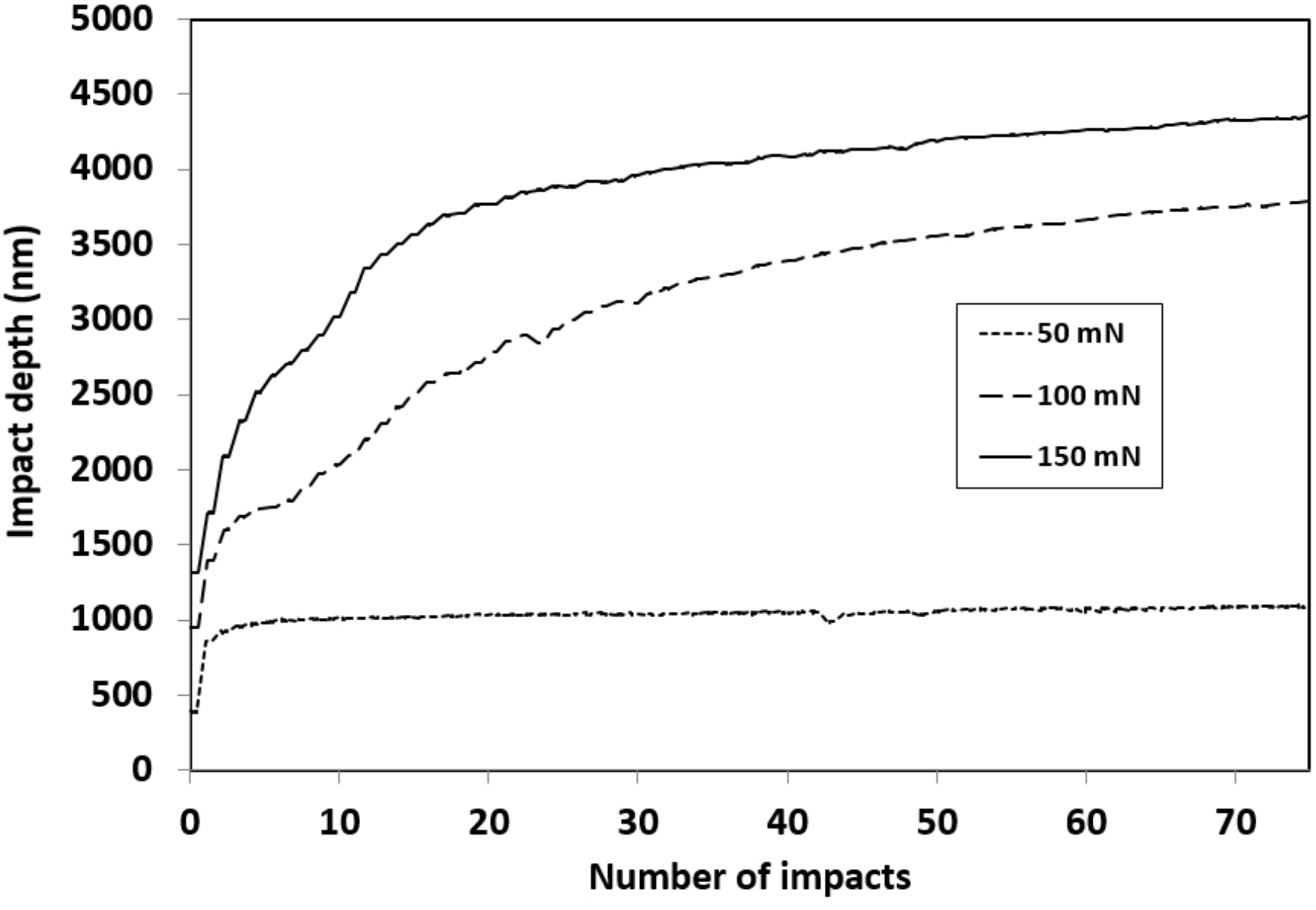
5000
4500
4000
3500
3000
2500
2000
1500
1000
500
0
Impact depth (nm)
0
10
20
30
40
50
60
70
Number of impacts
50 mN
100 mN
150 mN

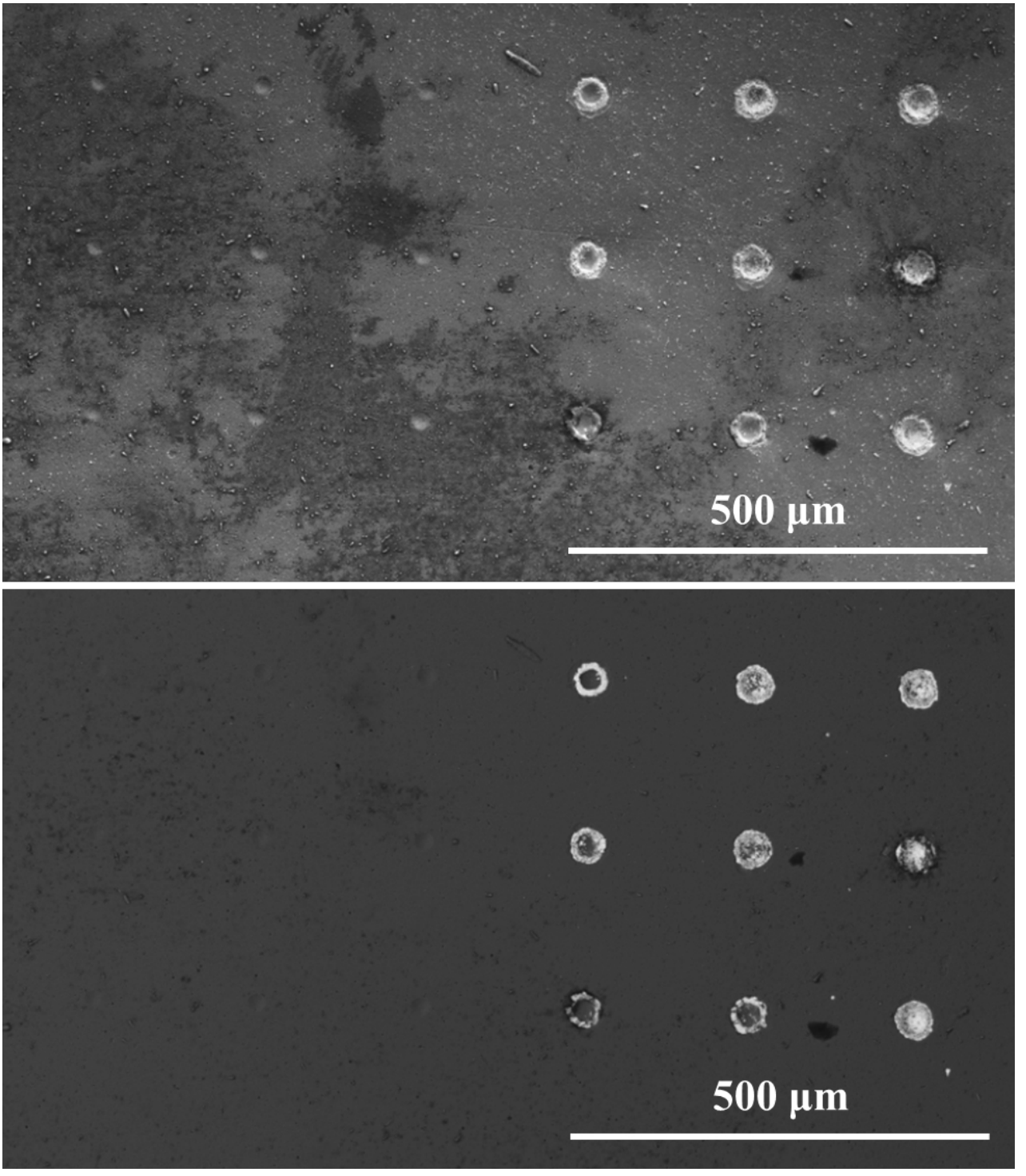
500 µm
500 µm

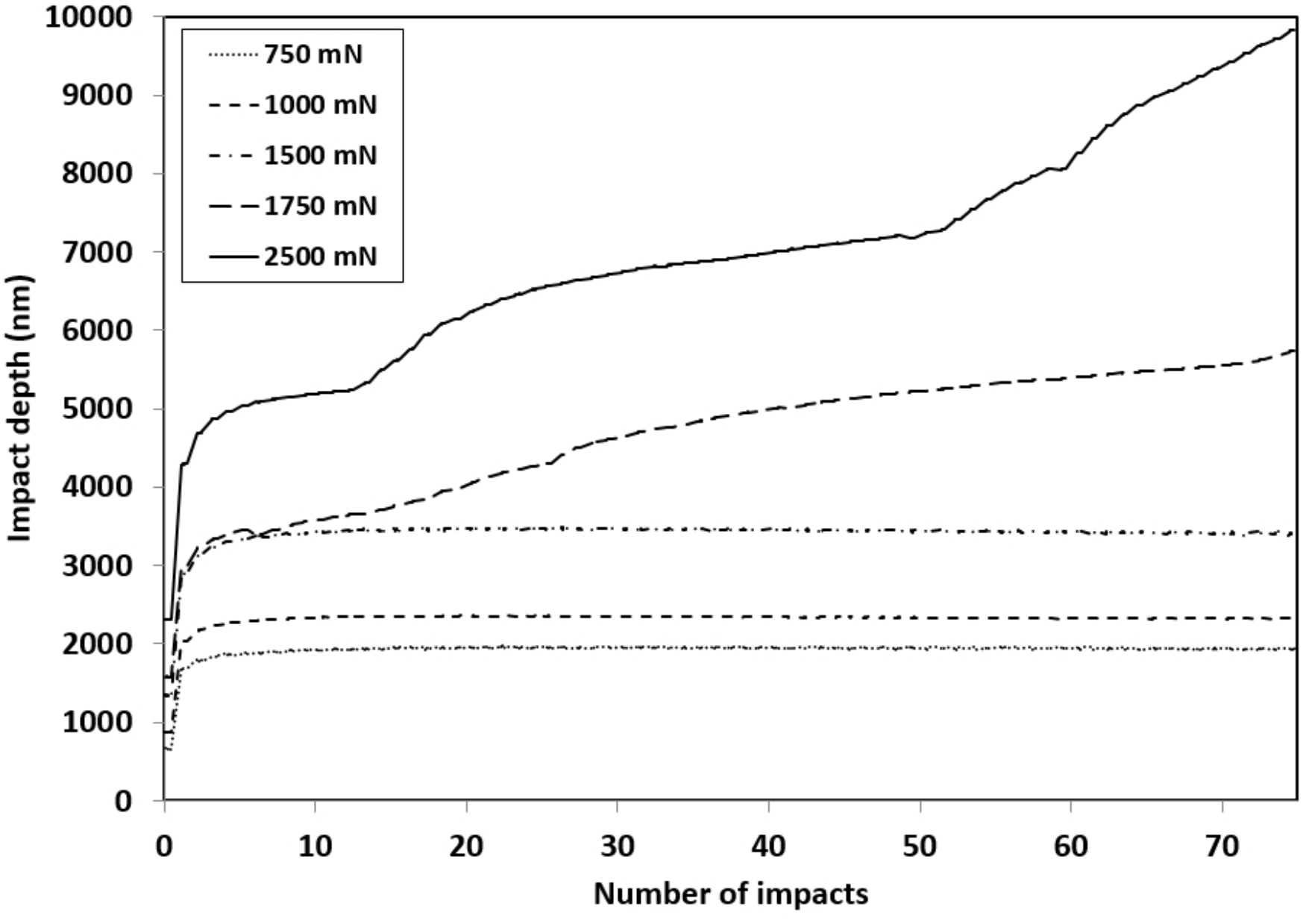
750 mN
1000 mN
1500 mN
1750 mN
2500 mN
Impact depth (nm)
0
1000
2000
3000
4000
5000
6000
7000
8000
9000
10000
0
10
20
30
40
50
60
70
Number of impacts

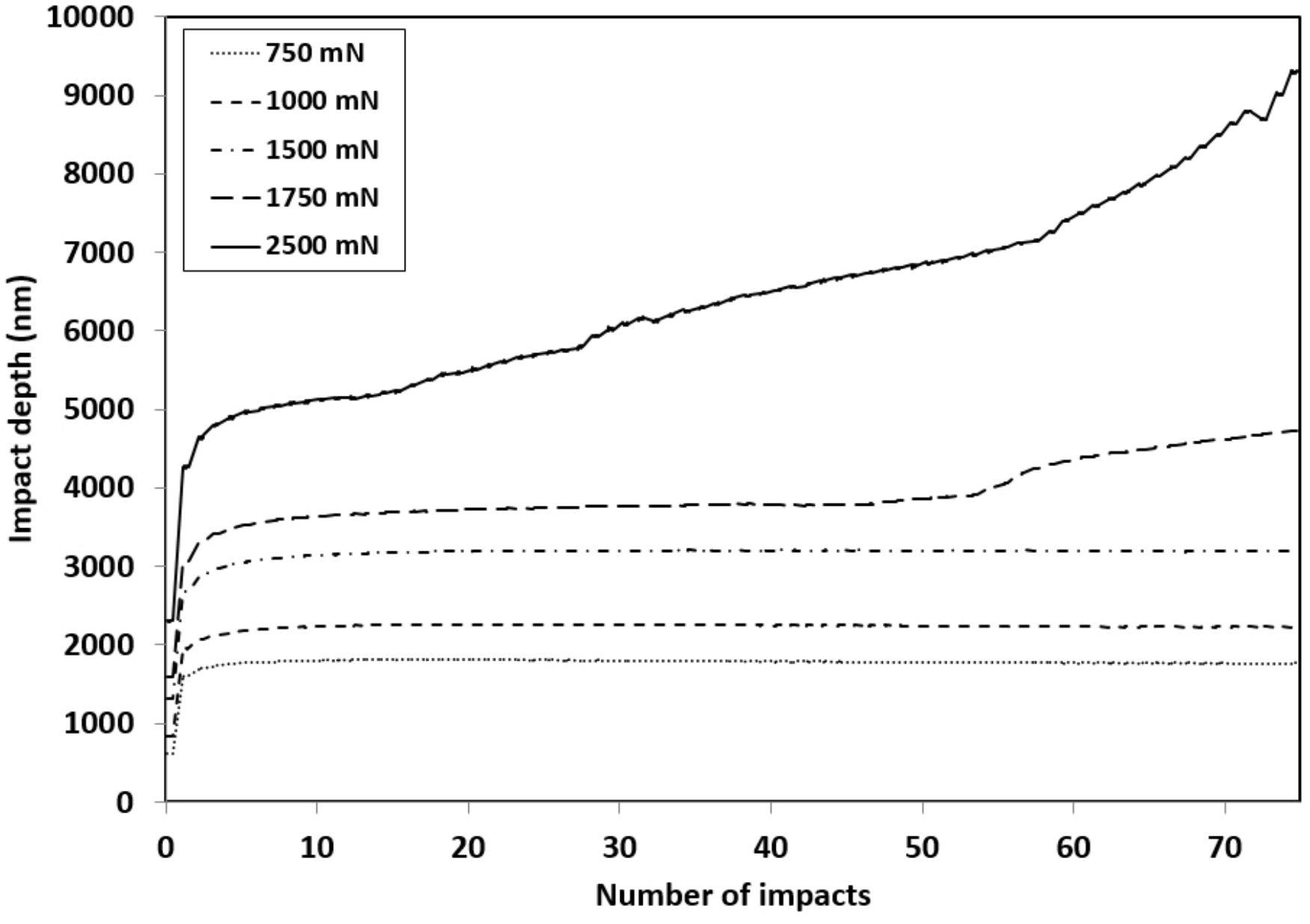
750 mN
1000 mN
1500 mN
1750 mN
2500 mN
Impact depth (nm)
10000
9000
8000
7000
6000
5000
4000
3000
2000
1000
0
0
10
20
30
40
50
60
70
Number of impacts

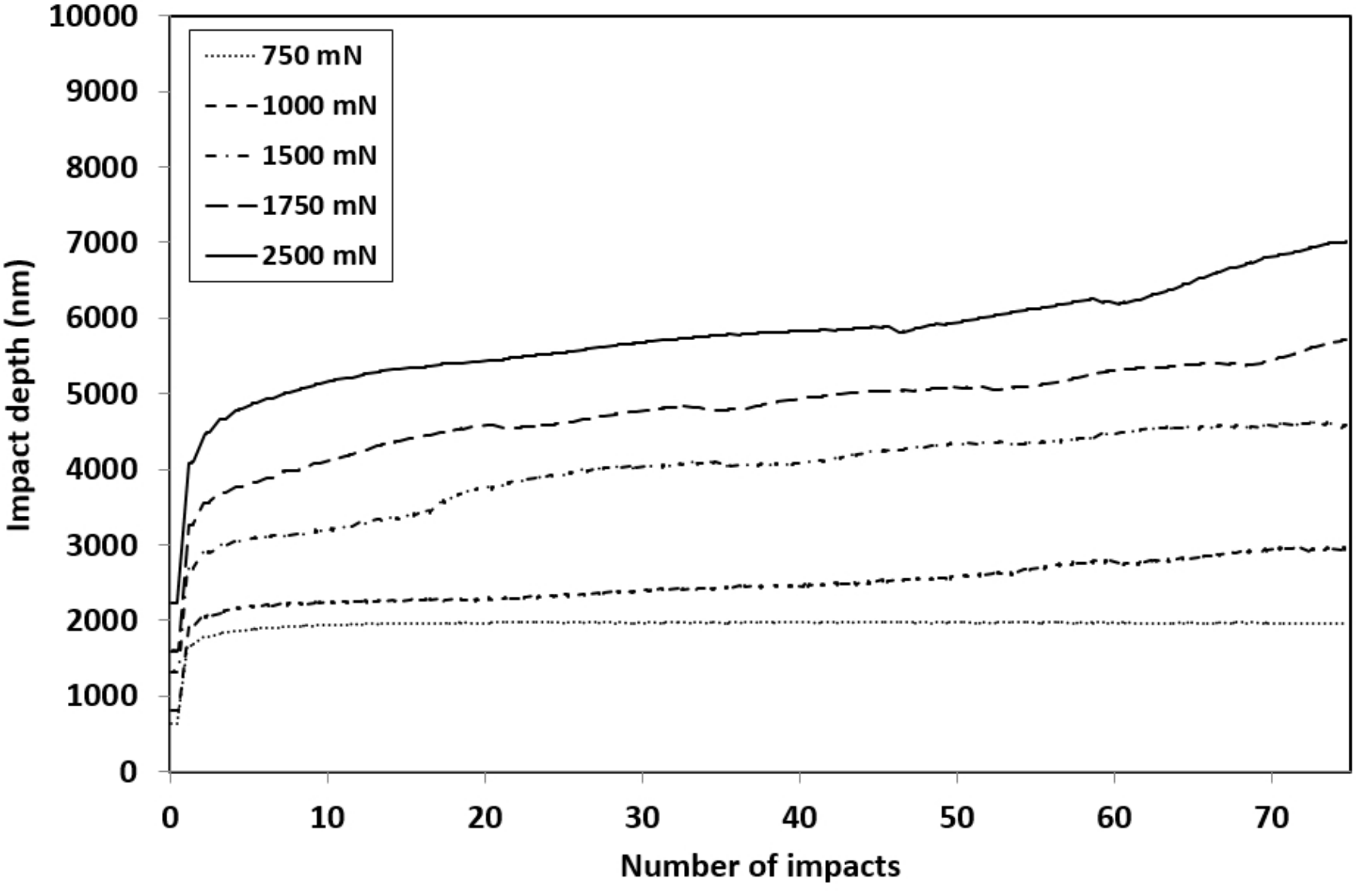
750 mN
1000 mN
1500 mN
1750 mN
2500 mN
Impact depth (nm)
10000
9000
8000
7000
6000
5000
4000
3000
2000
1000
0
0
10
20
30
40
50
60
70
Number of impacts

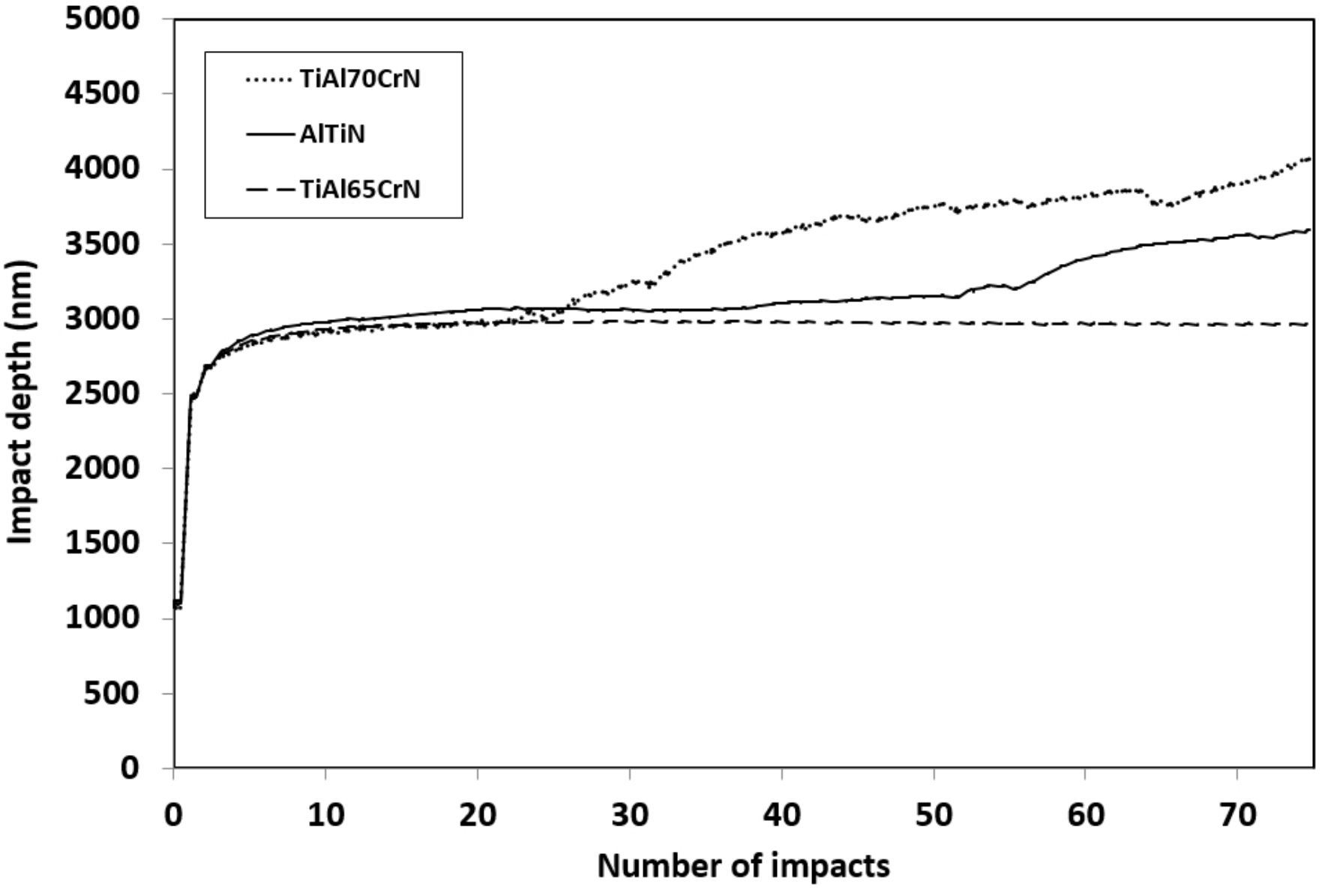
TiAl70CrN
AlTiN
TiAl65CrN
Impact depth (nm)
5000
4500
4000
3500
3000
2500
2000
1500
1000
500
0
0
10
20
30
40
50
60
70
Number of impacts

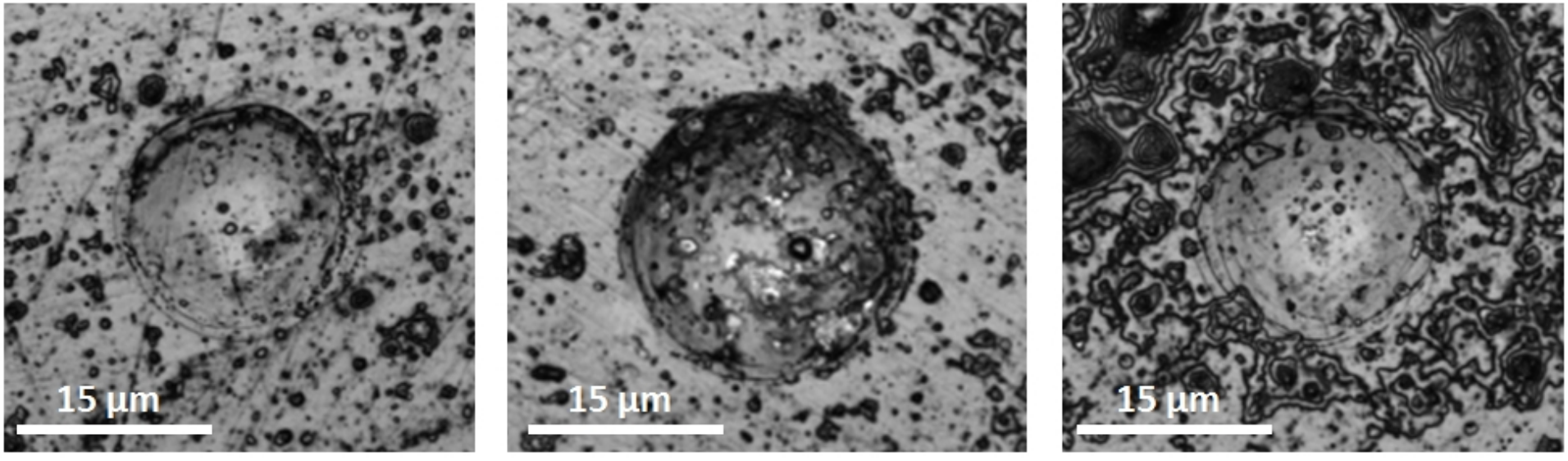
15 µm
15 µm
15 µm

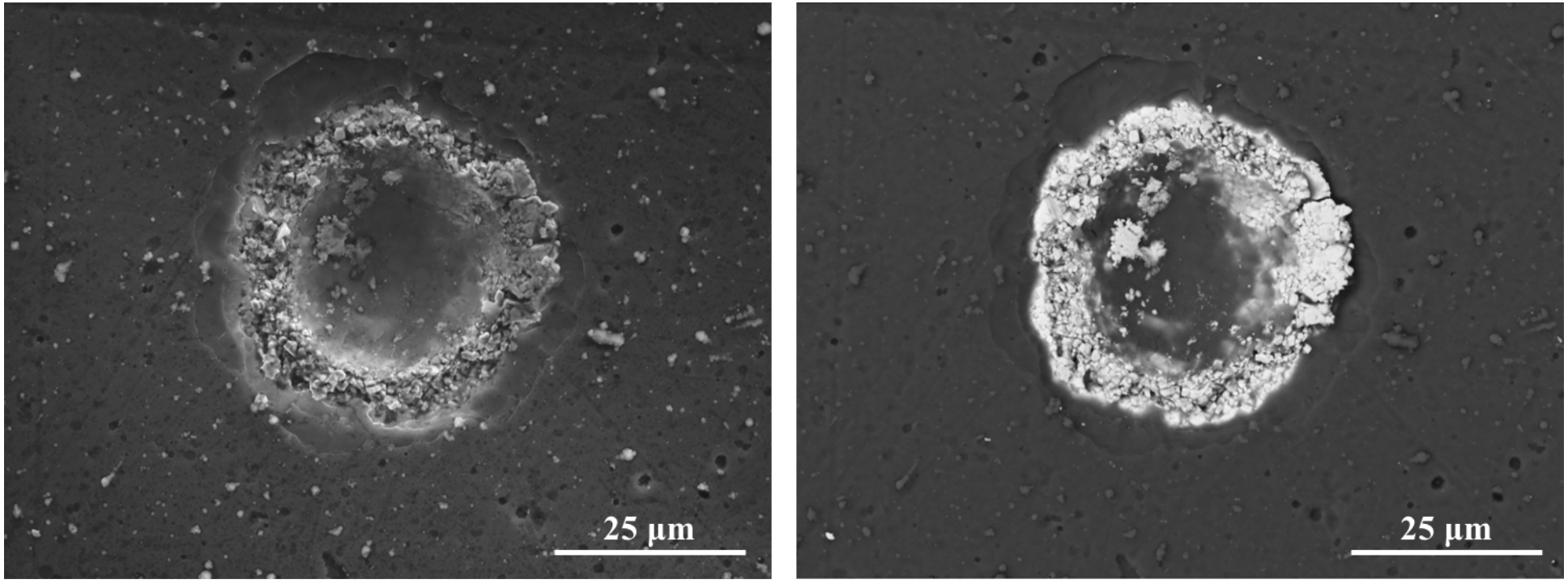
25 µm
25 µm

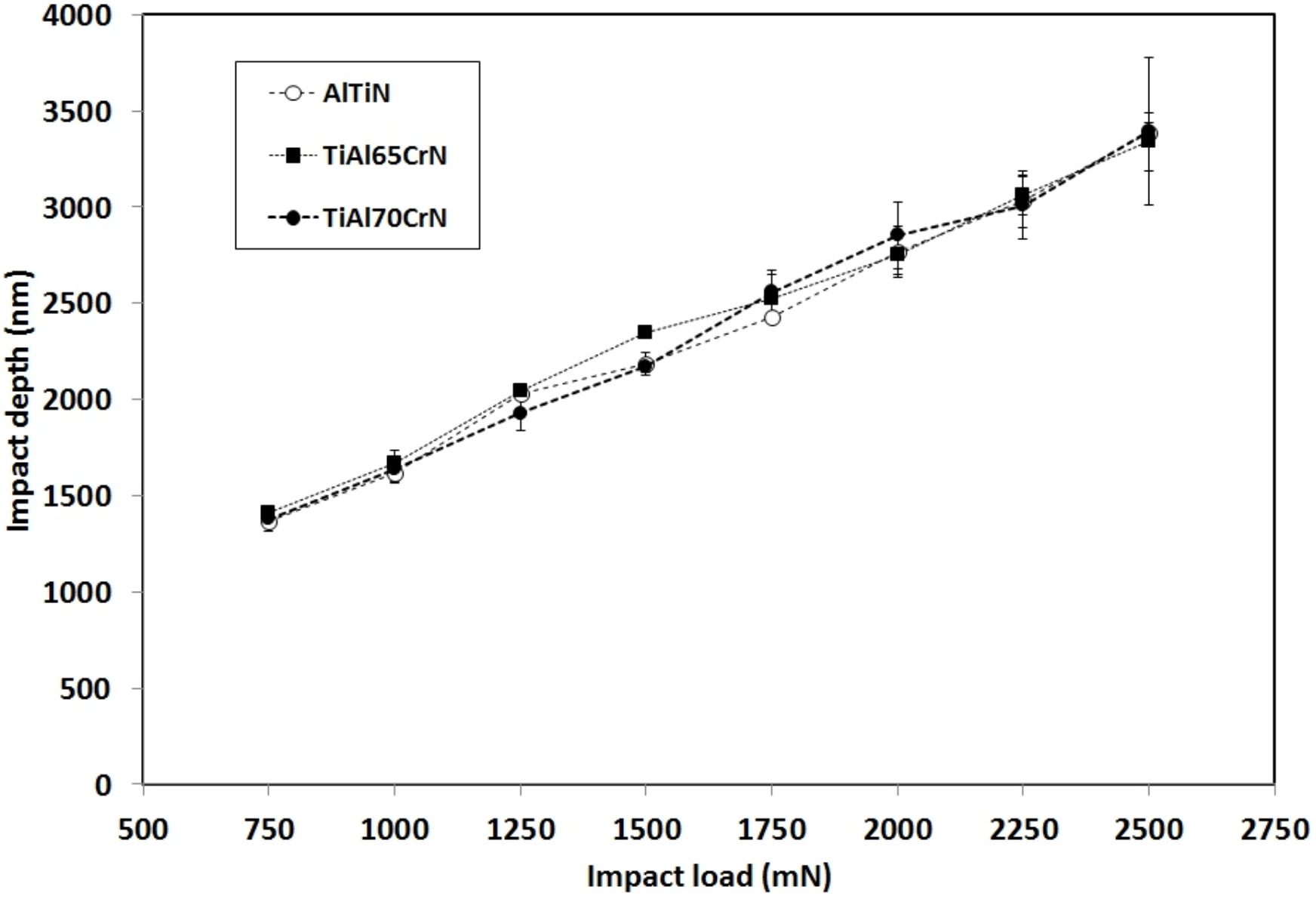
AlTiN
TiAl65CrN
TiAl70CrN
Impact depth (nm)
Impact load (mN)
0
500
1000
1500
2000
2500
3000
3500
4000
500
750
1000
1250
1500
1750
2000
2250
2500
2750

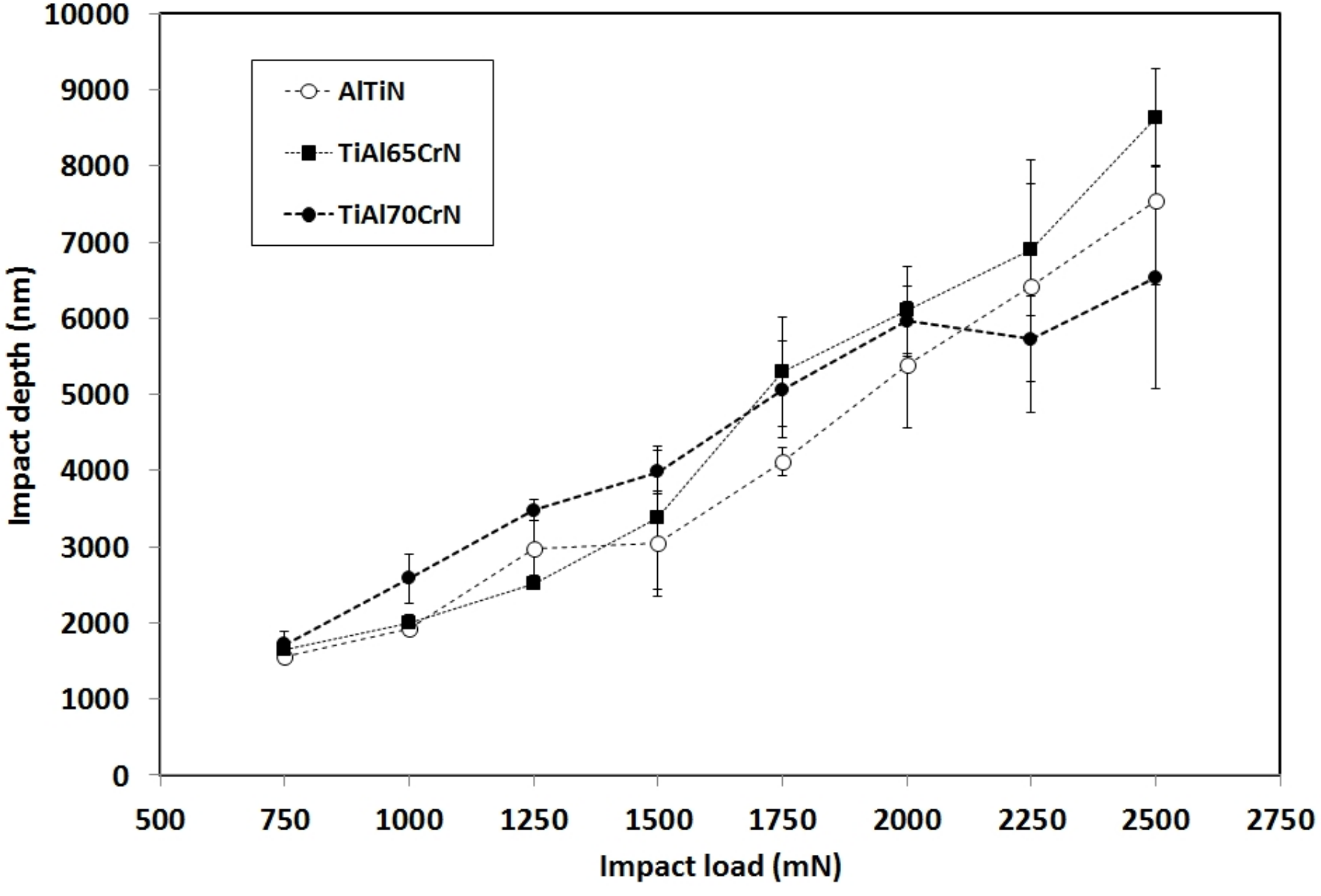
AlTiN
TiAl65CrN
TiAl70CrN
Impact depth (nm)
0
1000
2000
3000
4000
5000
6000
7000
8000
9000
10000
500
750
1000
1250
1500
1750
2000
2250
2500
2750
Impact load (mN)

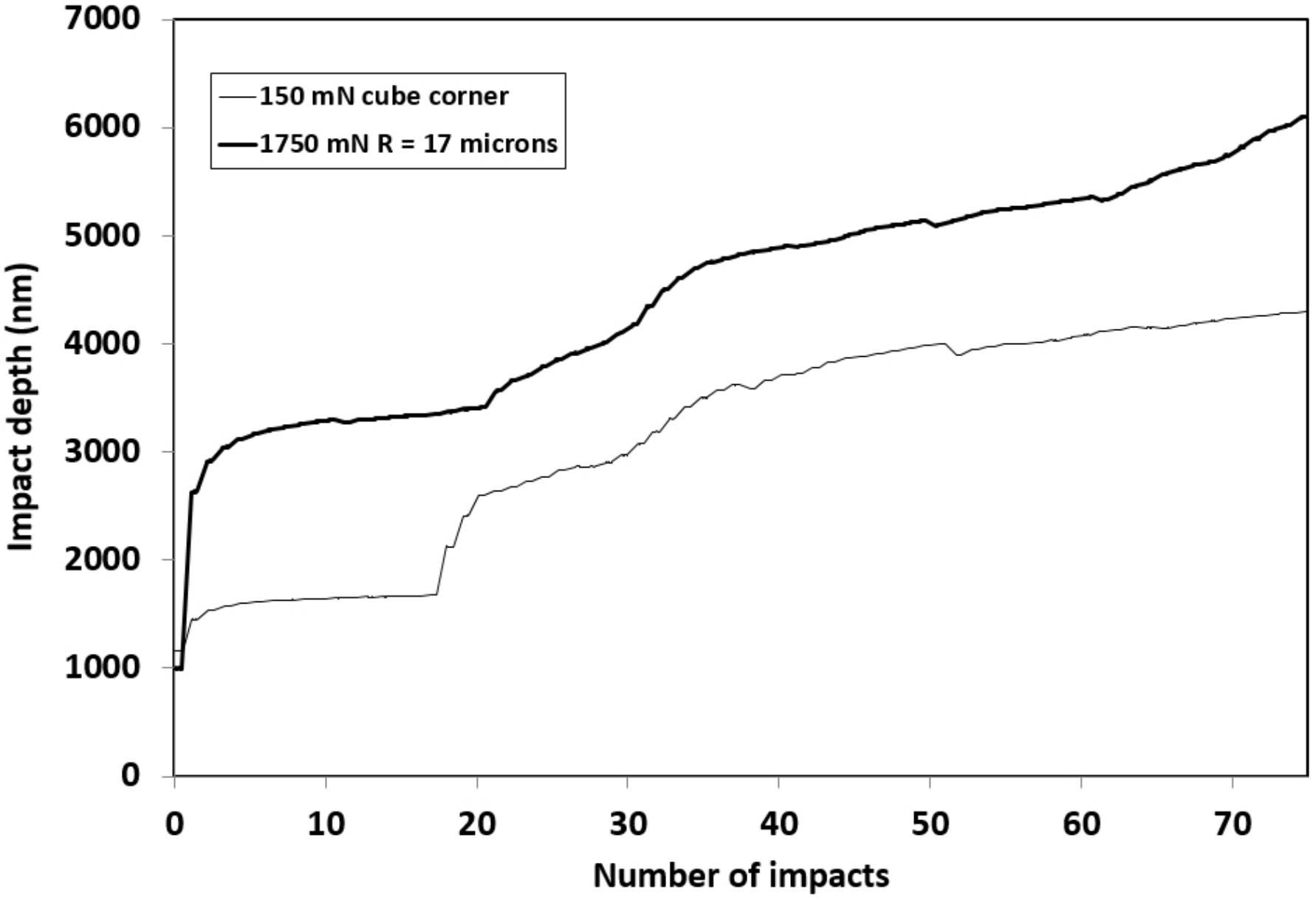
150 mN cube corner
1750 mN R = 17 microns
Impact depth (nm)
7000
6000
5000
4000
3000
2000
1000
0
0
10
20
30
40
50
60
70
Number of impacts